Electronic Supporting Information

Functionalized tris(anilido)triazacyclononanes as hexadentate ligands for the encapsulation of U(III), U(IV) and La(III) cations

Alasdair Formanuik[1], Fabrizio Ortu[1,2], Iñigo. J. Vitorica-Yrezabal[1], Floriana Tuna[1], Eric J. L. McInnes[1], Louise S. Natrajan[1,*] and David P. Mills[1,*]

[1] Department of Chemistry; The University of Manchester, Oxford Road, Manchester, M13 9PL, U.K. aformanuik@outlook.com (A.F.); inigo.vitorica@manchester.ac.uk (I.J.V-Y.); floriana.tuna@manchester.ac.uk (F.T.); eric.mcinnes@manchester.ac.uk (E.J.L.M.).

[2] School of Chemistry, University of Leicester, University Road, Leicester, LE1 7RH, U.K.; fabrizio.ortu@leicester.ac.uk.

***** Correspondence: louise.natrajan@manchester.ac.uk; david.mills@manchester.ac.uk; Tel.: +44-161-275-4606

Contents

S1. Crystallographic details

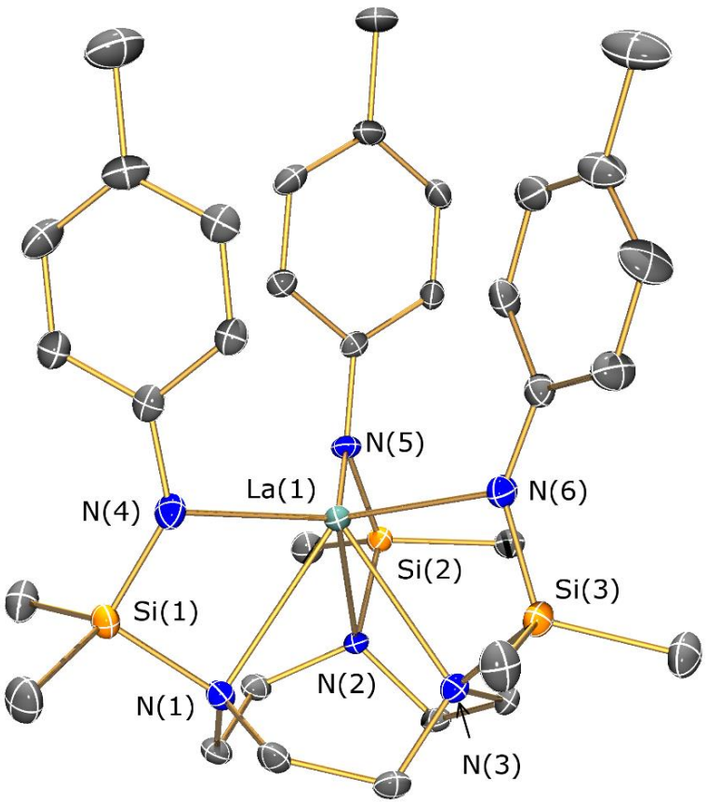

Figure S1. Molecular structure of [La{tacn(SiMe$_2$NC$_6$H$_4$Me-4)$_3$}] (**3-La·0.5C$_7$H$_8$**) with selective atom labelling. Displacement ellipsoids set at 30% probability level and hydrogen atoms and lattice toluene omitted for clarity.

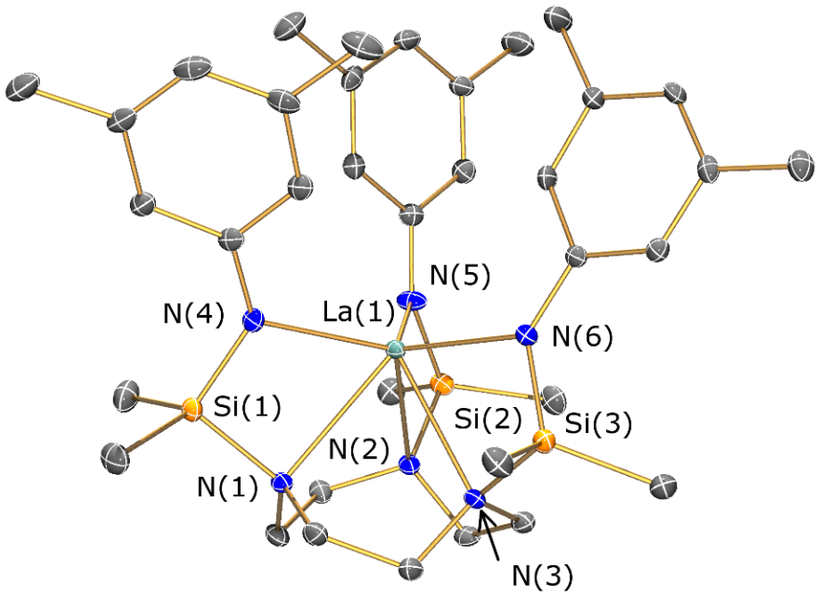

Figure S2. Molecular structure of [La{tacn(SiMe$_2$NC$_6$H$_3$Me$_2$-3,5)$_3$}] (**4-La**) with selective atom labelling. Displacement ellipsoids set at 30% probability level and hydrogen atoms omitted for clarity.

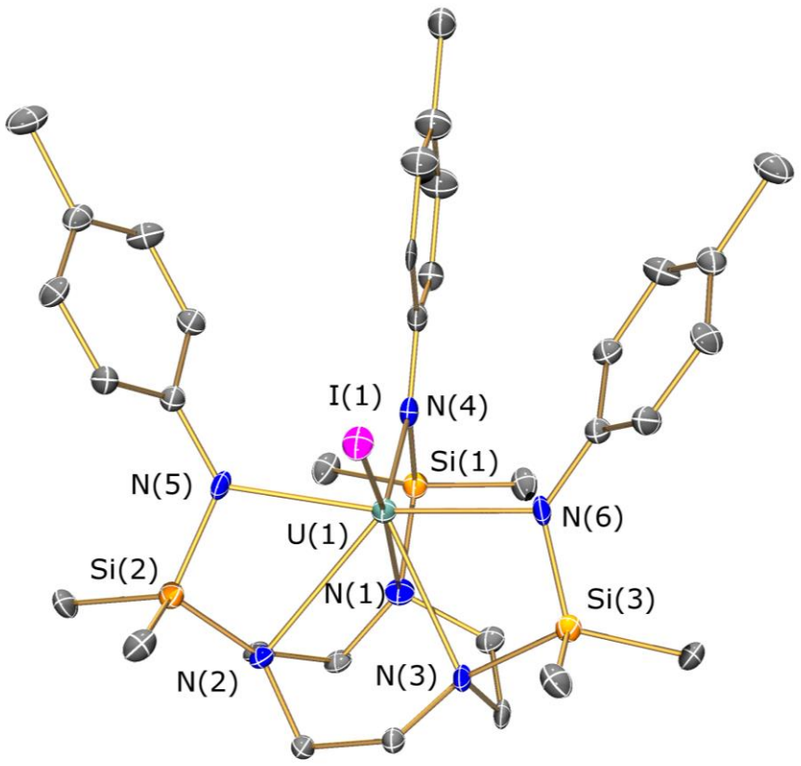

Figure S3. Molecular structure of [U{tacn(SiMe$_2$NC$_6$H$_4$Me-4)$_3$}(I)] (**5**) with selective atom labelling. Displacement ellipsoids set at 30% probability level and hydrogen atoms omitted for clarity.

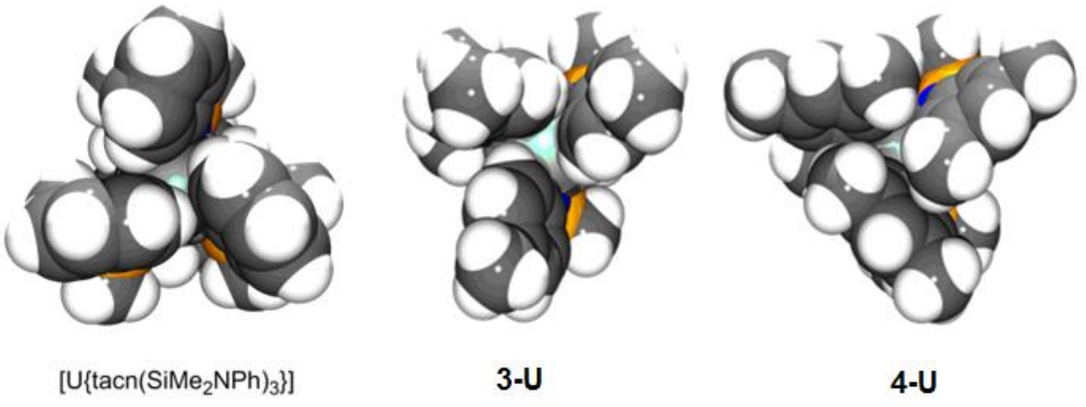

Figure S4. Space-filling representations of [U{tacn(SiMe$_2$NPh)$_3$}], **3-U** and **4-U** viewed along the approximate *C*$_3$ axes above the *N*-aryl rings (U: cyan, C: grey, H: white, N: blue, Si: coral).

Table S1. Crystallographic data for **3-La·0.5C_7H_8**, **3-U·0.5C_7H_8**, **4-La** and **4-U**.

	3-La·0.5C_7H_8	**3-U·0.5C_7H_8**	**4-La**	**4-U**
Formula	$C_{73}H_{110}La_2N_{12}Si_6$	$C_{73}H_{110}U_2N_{12}Si_6$	$C_{36}H_{57}LaN_6Si_3$	$C_{36}H_{57}UN_6Si_3$
Fw	1602.08	1800.32	797.05	896.17
crystal size, mm	0.06 x 0.10 x 0.13	0.02 x 0.06 x 0.18	0.09 x 0.15 x 0.23	0.04 x 0.12 x 0.13
crystal colour, habit	colourless, block	red, block	yellow, block	red, block
crystal system	triclinic	triclinic	monoclinic	monoclinic
space group	*P*–1	*P*–1	$P2_1/n$	$P2_1/n$
a, Å	12.4192(4)	12.4091(6)	12.0915(3)	12.0318(14)
b, Å	18.3391(6)	18.2810(8)	16.1964(4)	16.230(5)
c, Å	18.7396(6)	18.8018(8)	20.9440(5)	20.906(2)
α, °	66.758(3)	66.874(4)	90	90
β, °	87.521(3)	87.407(4)	103.91(2)	103.947(11)
γ, °	87.639(3)	87.821(4)	90	90
V, Å^3	3916.7(2)	3917.5(3)	3981.5(2)	3962.1(14)
Z	2	2	4	4
ρ_{calcd}, g cm^3	0.597	0.724	1.234	1.406
μ, mm^{-1}	1.215	4.268	1.195	4.220
F(*000*)	678	850	1428	1568
no. of reflections (unique)	21879 (14193)	22195 (14209)	16679 (7288)	12818 (7216)
S[a]	1.02	1.02	1.04	0.89
$R_1(wR_2)$ ($F^2 > 2\sigma(F^2)$)	0.0337(0.0679)	0.0655(0.1041)	0.0345(0.0714)	0.0868(0.1804)
no. of parameters (restraints)	857 (0)	857 (927)	427 (0)	427 (456)
R_{int}	0.025	0.067	0.034	0.179
min./max. diff map, Å^{-3}	–0.34, 0.38	–1.69, 1.51	–0.44, 0.42	–3.90, 3.89

[a] Conventional $R = \Sigma||F_o| - |F_c||/\Sigma|F_o|$; $R_w = [\Sigma w(F_o^2 - F_c^2)^2/\Sigma w(F_o^2)^2]^{1/2}$; $S = [\Sigma w(F_o^2 - F_c^2)^2/\text{no. data} - \text{no. params})]^{1/2}$ for all data.

Table S2. Crystallographic data for **5**, **6·THF** and **7**.

	5	**6·THF**	**7**
Formula	$C_{33}H_{51}IN_6Si_3U$	$C_{37}H_{59}ClON_6Si_3U$	$C_{96}H_{130}Cl_2N_{12}Si_6U_2$
Fw	980.99	961.65	2047.51
crystal size, mm	0.08 x 0.09 x 0.14	0.04 x 0.11 x 0.14	0.07 x 0.11 x 0.14
crystal colour, habit	red, block	red, block	red, block
crystal system	orthorhombic	monoclininc	orthorhombic
space group	*Pmn*2$_1$	*P*2$_1$/*c*	*Pnma*
a, Å	16.7641(15)	22.2114(9)	18.0078(9)
b, Å	9.1477(7)	8.8187(4)	15.5612(12)
c, Å	11.9248(11)	21.0934(9)	17.8903(8)
α, °	90	90	90
β, °	90	90.495(4)	90
γ, °	90	90	90
V, Å^3	1828.7(3)	4131.5(3)	5013.3(5)
Z	2	4	2
ρ_{calcd}, g cm^3	1.688	1.347	1.234
μ, mm^{-1}	5.412	4.117	3.396
F(*000*)	854	1564	1864
no. of reflections (unique)	4423 (2428)	12833 (7543)	11015 (4729)
S[a]	1.07	1.02	1.02
$R_1(wR_2)$ ($F^2 > 2\sigma(F^2)$)	0.0520(0.1322)	0.0649(0.1325)	0.0423 (0.0953)
no. of parameters (restraints)	258 (391)	470 (863)	350 (501)
R_{int}	0.051	0.093	0.048
min./max. diff map, Å^{-3}	–1.97, 2.13	–2.47, 2.46	–0.98, 1.15

[a] Conventional $R = \Sigma||F_o| - |F_c||/\Sigma|F_o|$; $R_w = [\Sigma w(F_o^2 - F_c^2)^2/\Sigma w(F_o^2)^2]^{1/2}$; $S = [\Sigma w(F_o^2 - F_c^2)^2/\text{no. data} - \text{no. params})]^{1/2}$ for all data.

S2. SQUID magnetometry

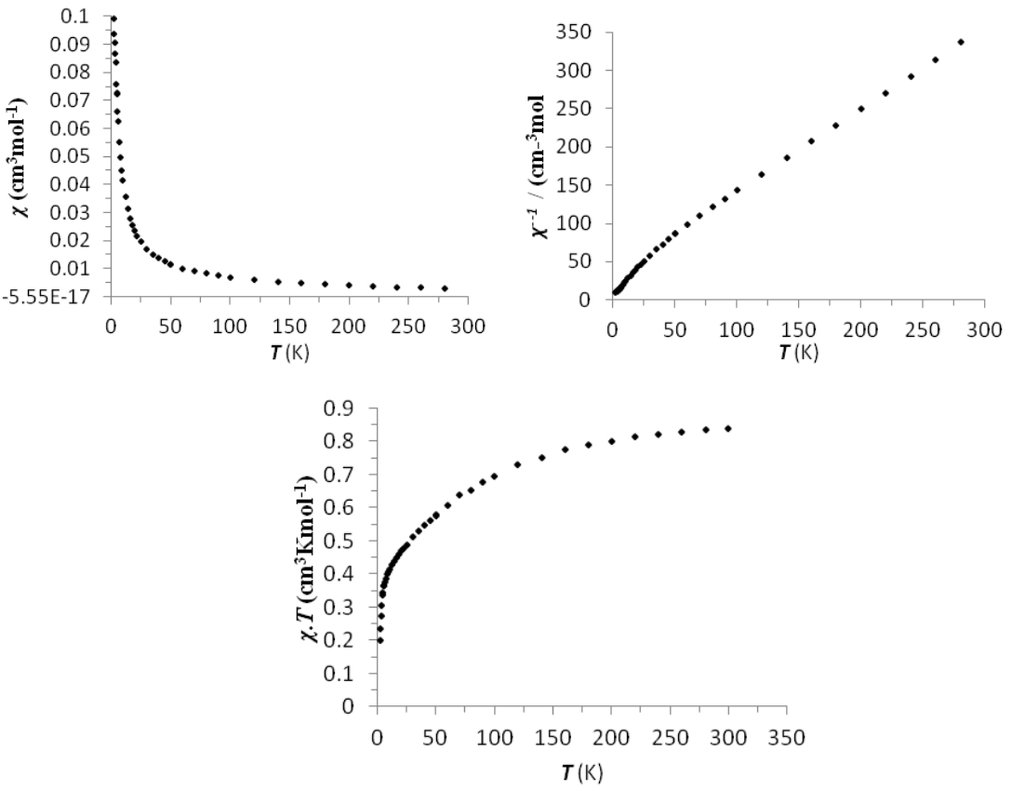

Figure S5. Magnetic measurements of **3-U**: (top left) Temperature dependence of susceptibility (χ); (top right) Temperature dependence of reciprocal susceptibility (χ′); (bottom) Temperature dependence of χT in a 5 kG applied field.

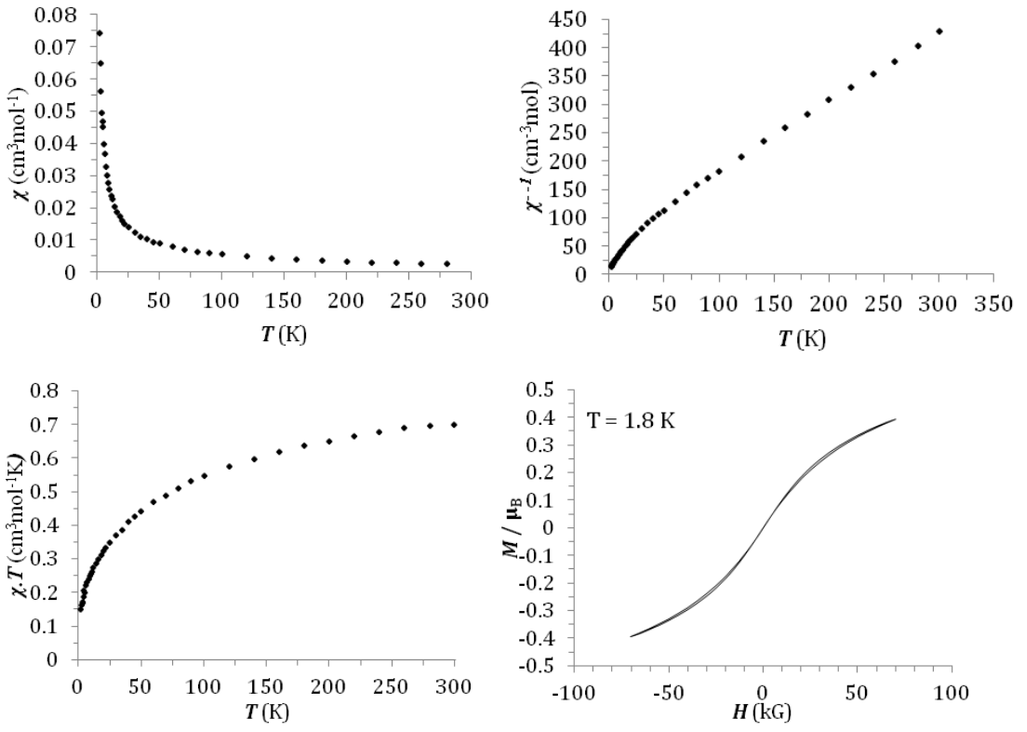

Figure S6. Magnetic measurements of **4-U**: (top left) Temperature dependence of susceptibility (χ); (top right) Temperature dependence of reciprocal susceptibility (χ′); (bottom left) Temperature dependence of χT in a 5 kG applied field; (bottom right) Magnetisation hysteresis at 1.8 K, sweep rate 13 G s^{-1}.

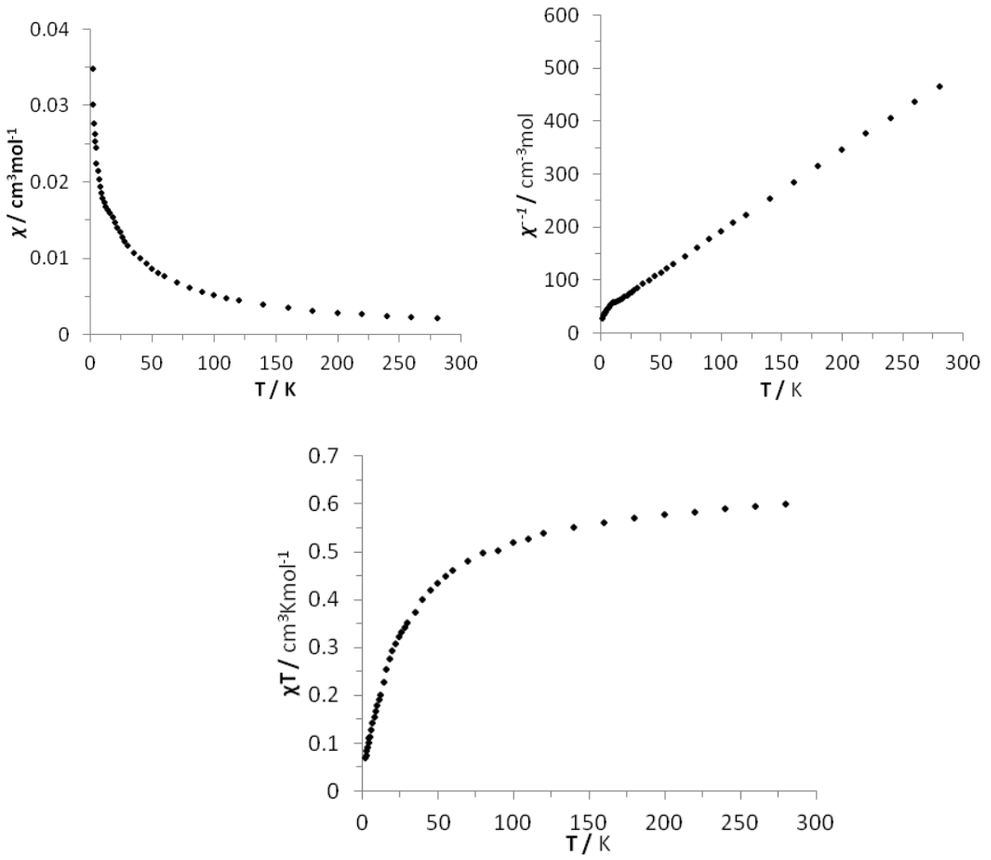

Figure S7. Magnetic measurements of **6**: (top left) Temperature dependence of susceptibility (χ); (top right) Temperature dependence of reciprocal susceptibility (χ′); (bottom) Temperature dependence of χT in a 5 kG applied field.

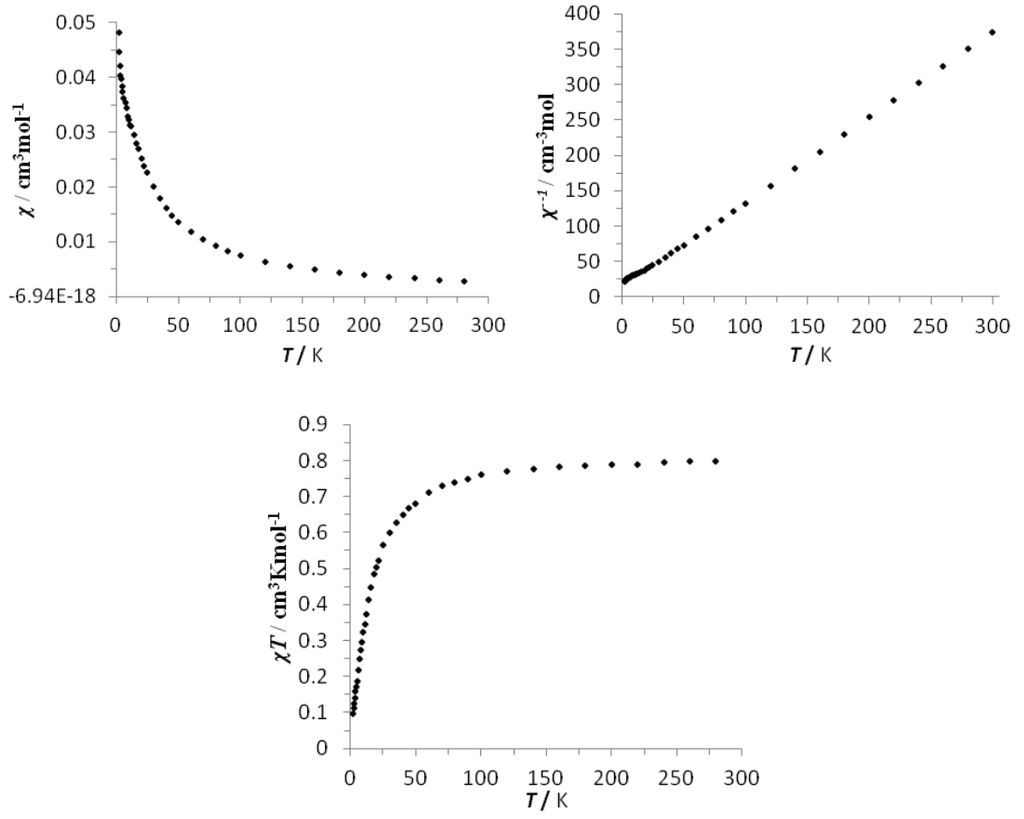

Figure S8. Magnetic measurements of **7**: (top left) Temperature dependence of susceptibility (χ); (top right) Temperature dependence of reciprocal susceptibility (χ′); (bottom) Temperature dependence of χT in a 5 kG applied field.

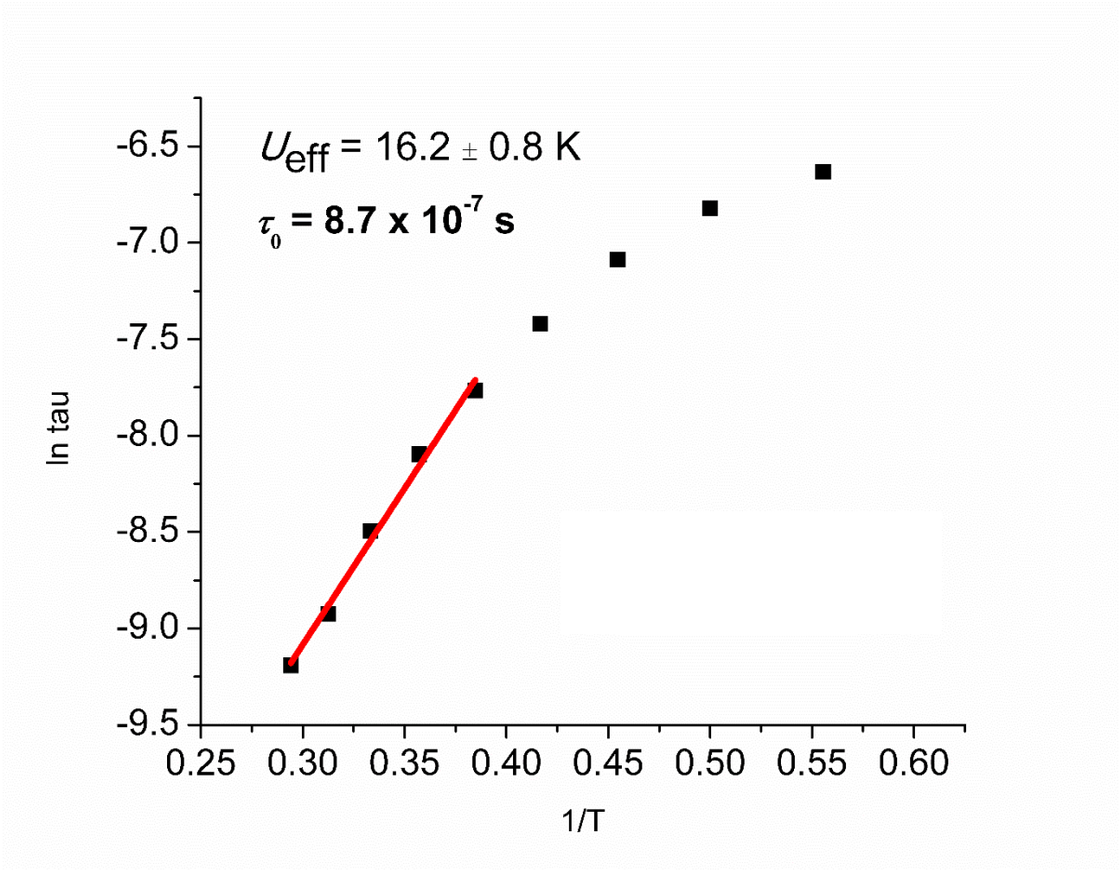

Figure S9. Arrhenius plot of **4-U**: (top left) Temperature dependence of susceptibility (χ); (top right) Temperature dependence of reciprocal susceptibility (χ′); (bottom) Temperature dependence of χT in a 5 kG applied field.

S3. EPR spectroscopy

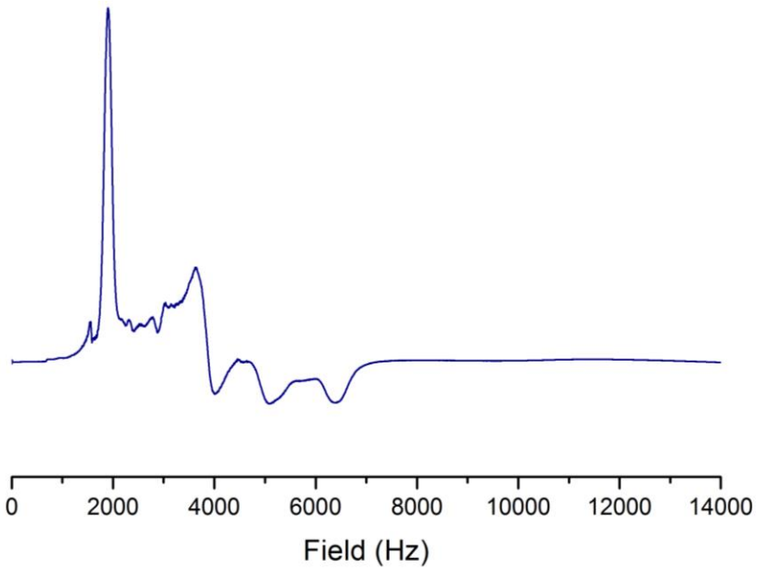

Figure S10. Powder X-band EPR spectra of **3-U** at 5 K.

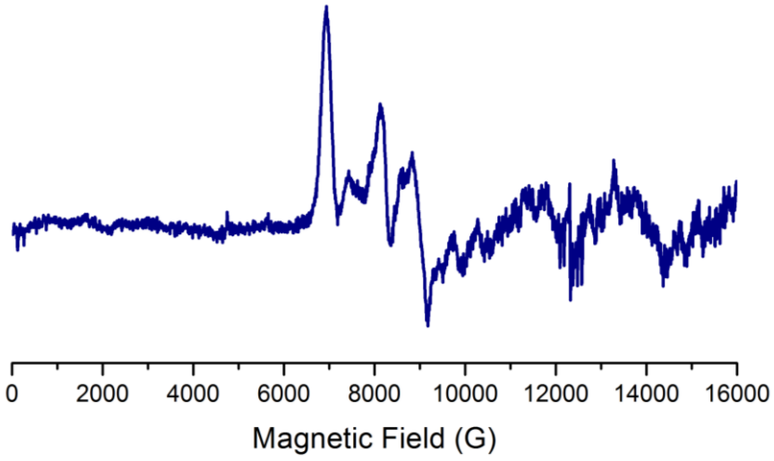

Figure S11. Powder Q-band EPR spectrum of **3-U** at 5 K.

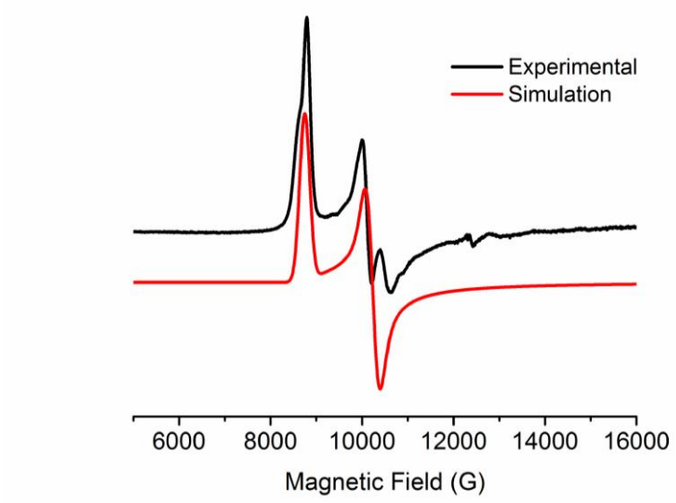

Figure S12. (black) Powder Q-band EPR spectrum of **4-U** at 5 K, and (red) its simulation with g_{eff} = 2.80, 2.37, 1.17 (the latter component is not observed at this m.w. frequency but was fixed based on X-band data).

S4. NMR spectroscopy

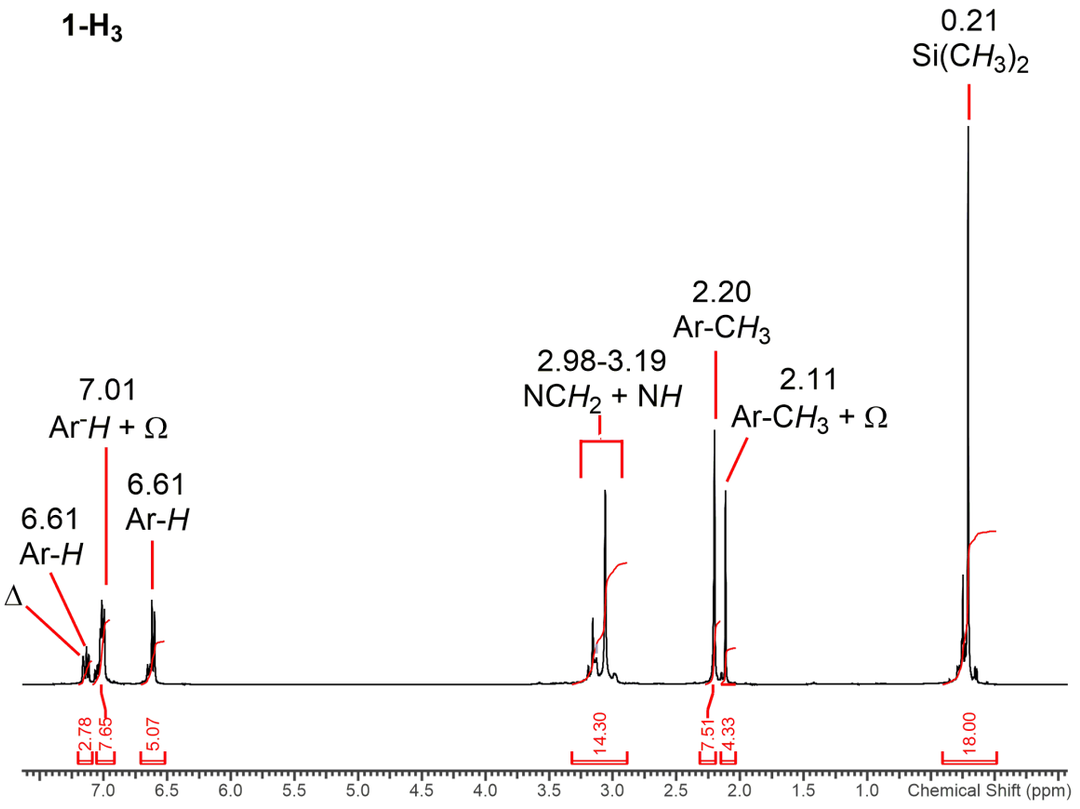

Figure S13. ^{1}H NMR spectrum of **1-H$_3$** in C_6D_6. Δ denotes C_6H_6 and Ω denotes residual C_7H_8.

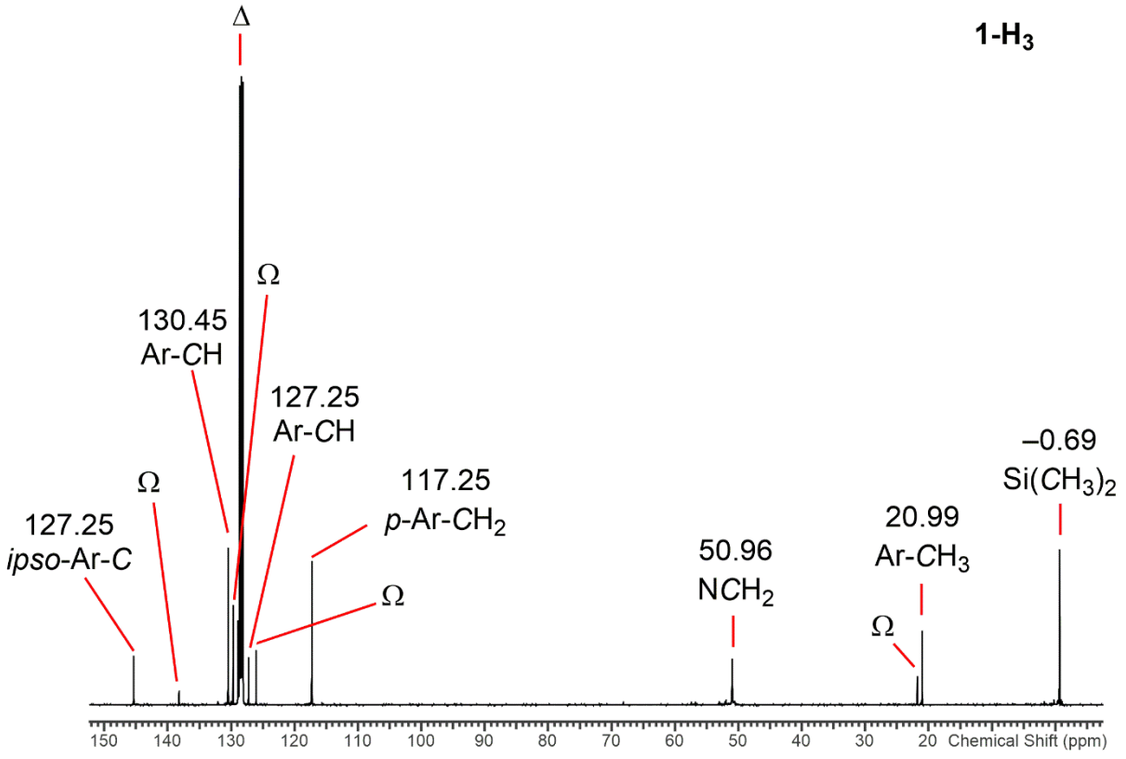

Figure S14. ^{13}C{^{1}H} NMR spectrum of **1-H$_3$** in C_6D_6. Δ denotes C_6H_6 and Ω denotes residual C_7H_8.

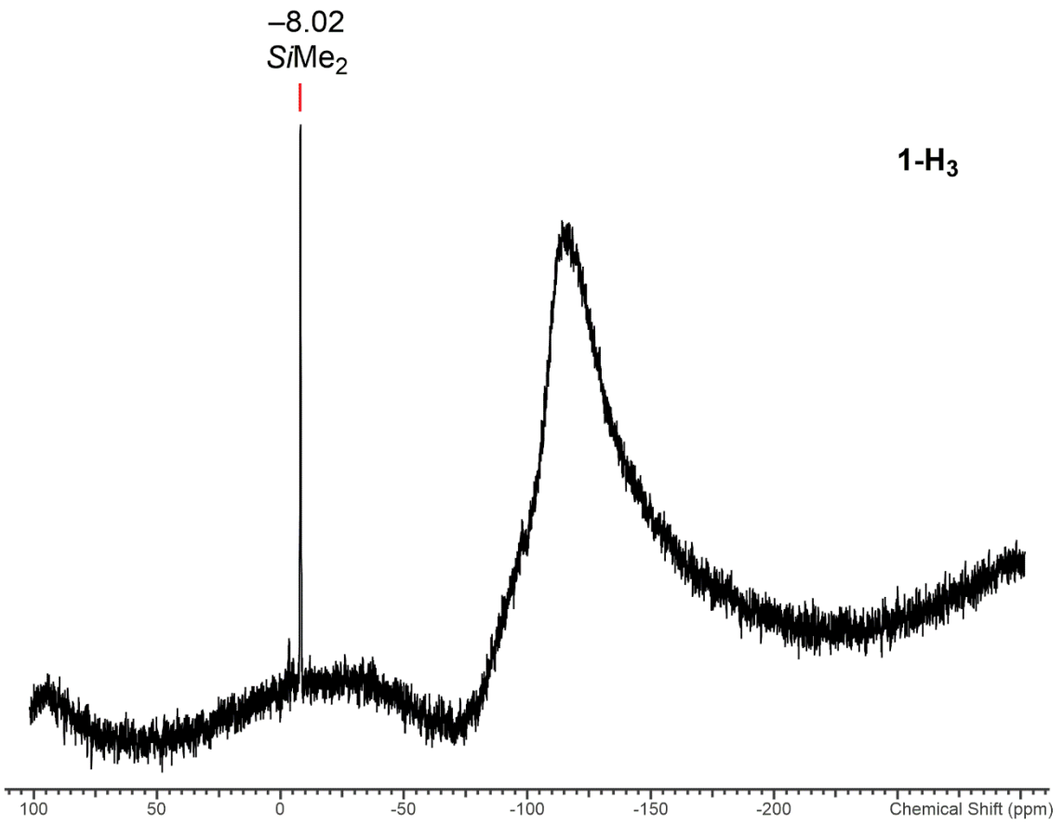

Figure S15. $^{29}Si\{^{1}H\}$ NMR spectrum of **1-H$_3$** in C_6D_6.

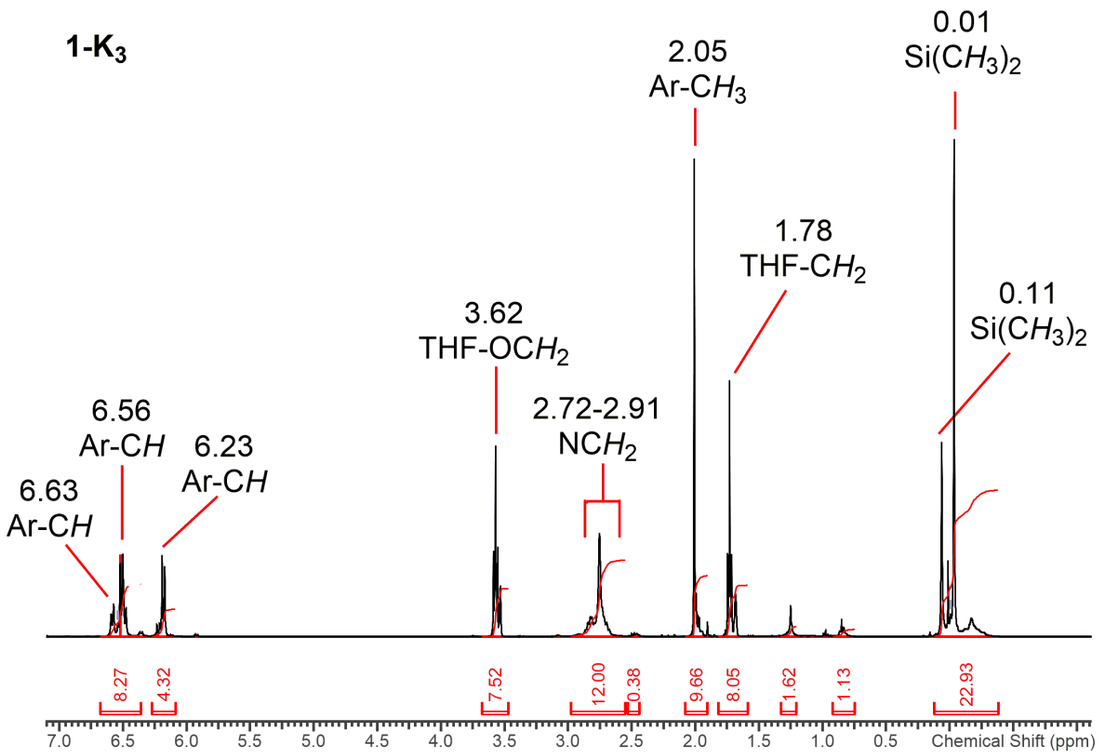

Figure S16. ^{1}H NMR spectrum of **1-K$_3$** in C_4D_8O.

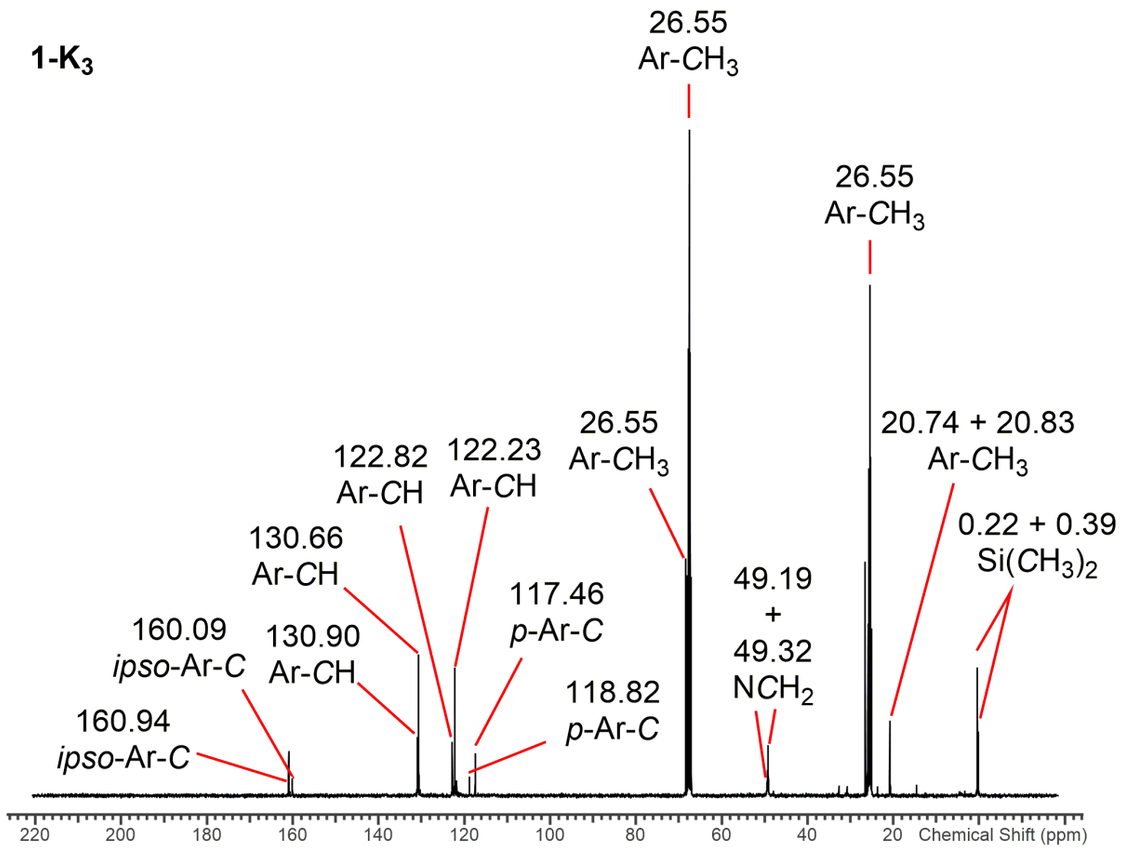

Figure S17. $^{13}C\{^{1}H\}$ NMR spectrum of **1-K$_3$** in C_4D_8O.

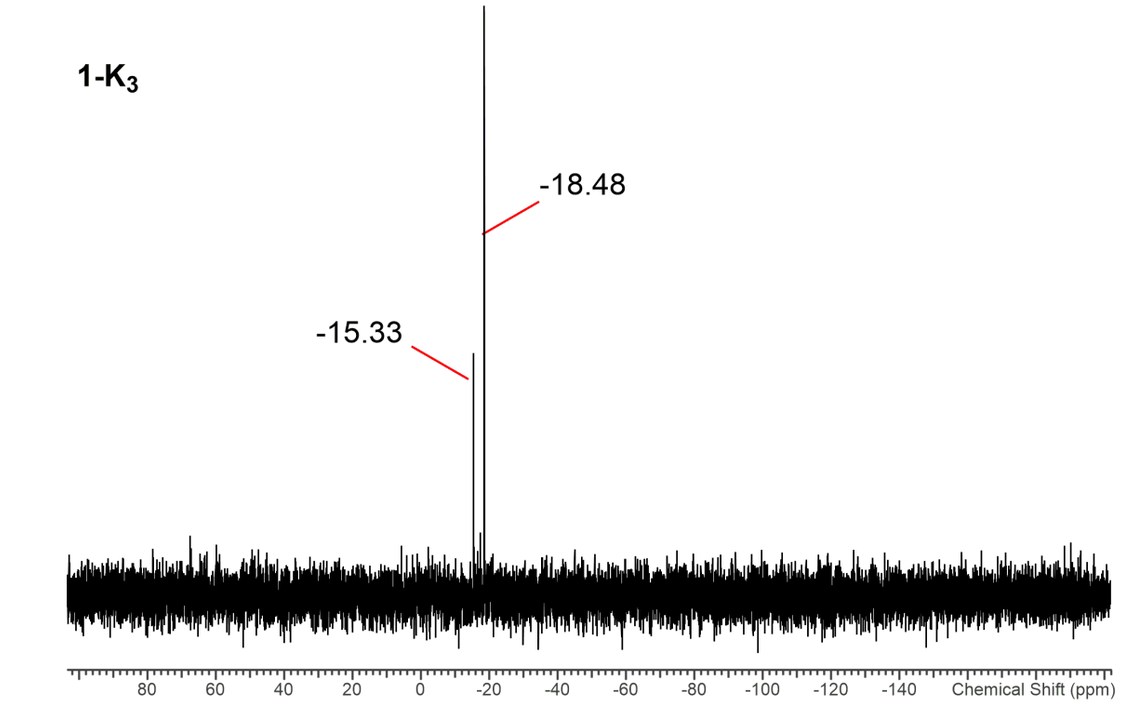

Figure S18. ^{29}Si DEPT NMR spectrum of **1-K$_3$** in C_4D_8O.

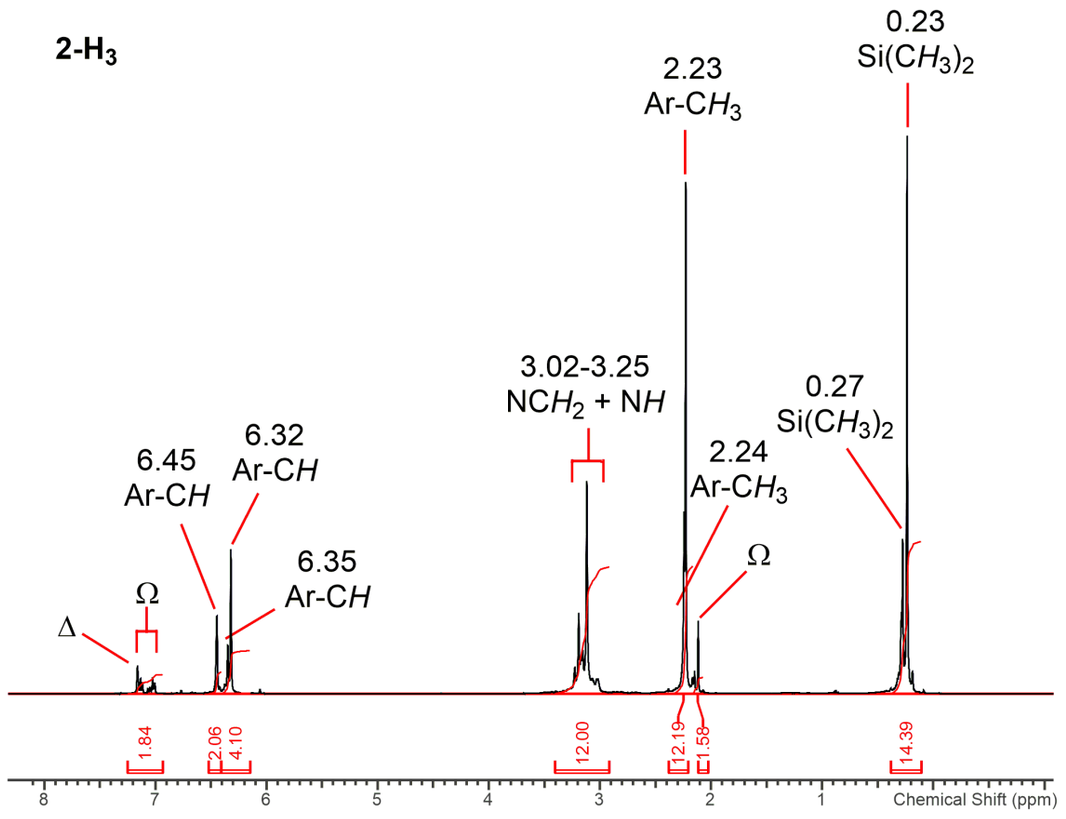

Figure S19. ^{1}H NMR spectrum of **2-H$_3$** in C_6D_6. Δ denotes C_6H_6 and Ω denotes residual C_7H_8.

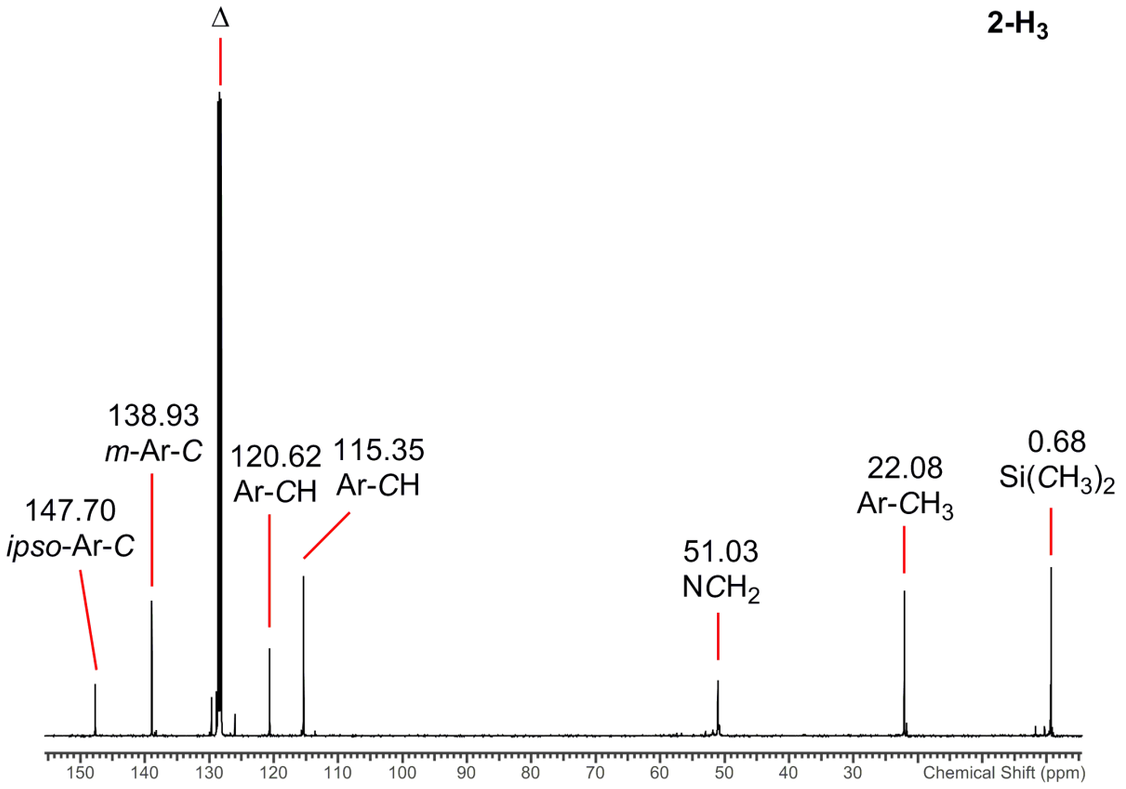

Figure S20. ^{13}C{^{1}H} NMR spectrum of **2-H$_3$** in C_6D_6. Δ denotes residual C_6H_6.

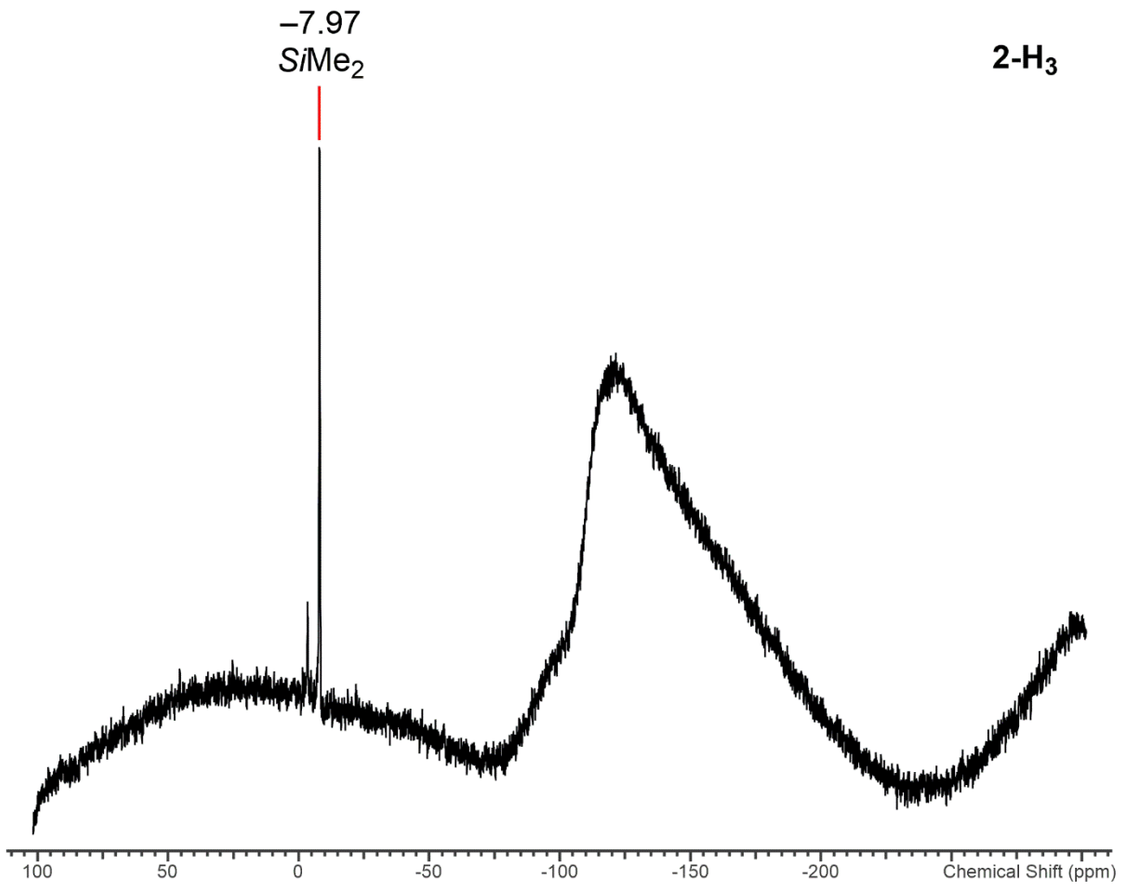

Figure S21. $^{29}Si\{^{1}H\}$ NMR spectrum of **2-H$_3$** in C_6D_6.

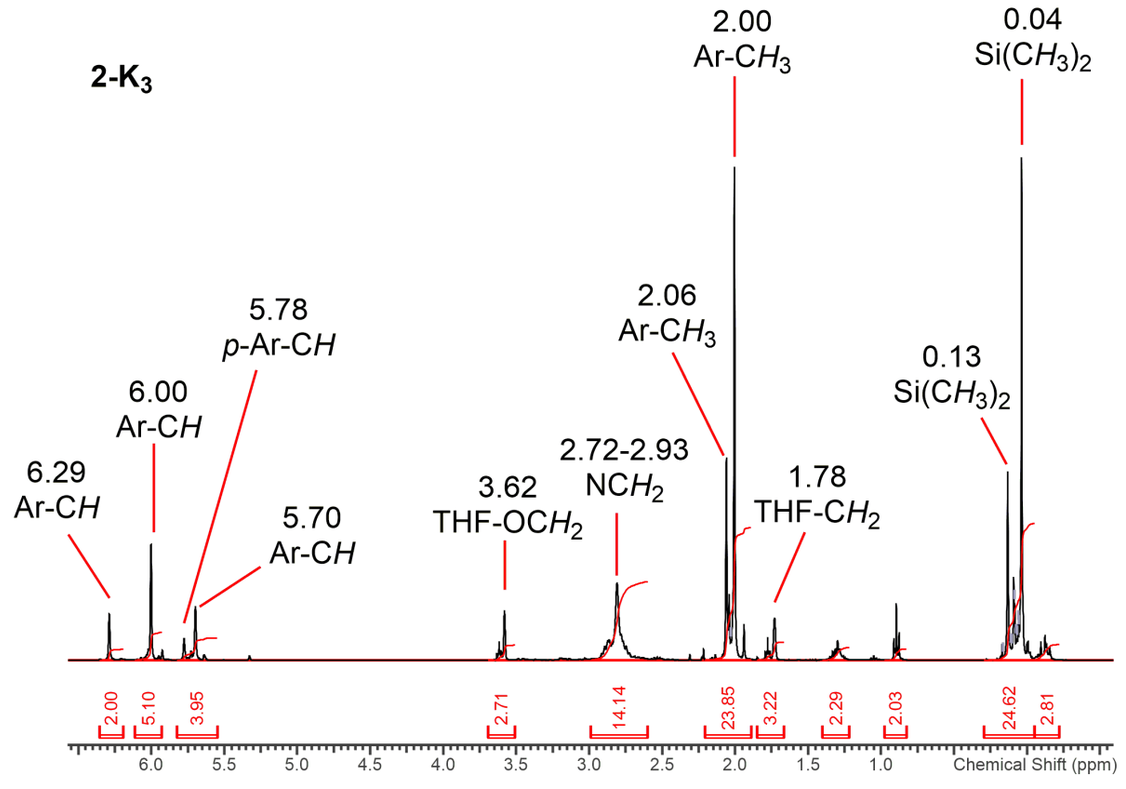

Figure S22. ^{1}H NMR spectrum of **2-K$_3$** in C_4D_8O.

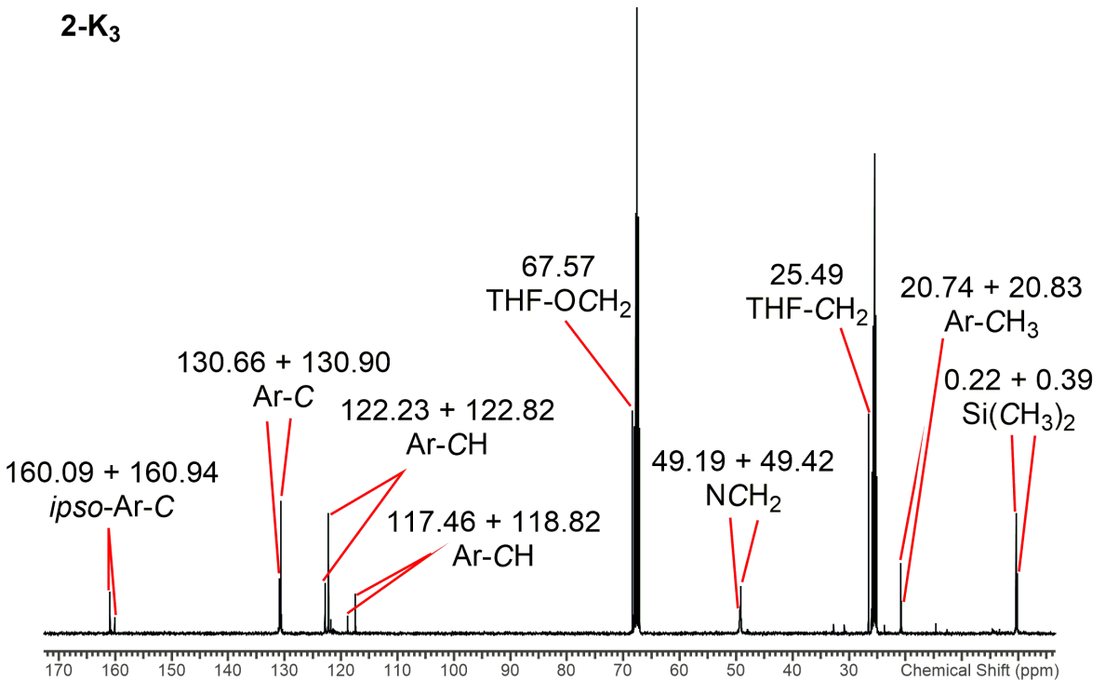

Figure S23. $^{13}C\{^{1}H\}$ NMR spectrum of **2-K$_3$** in C_4D_8O.

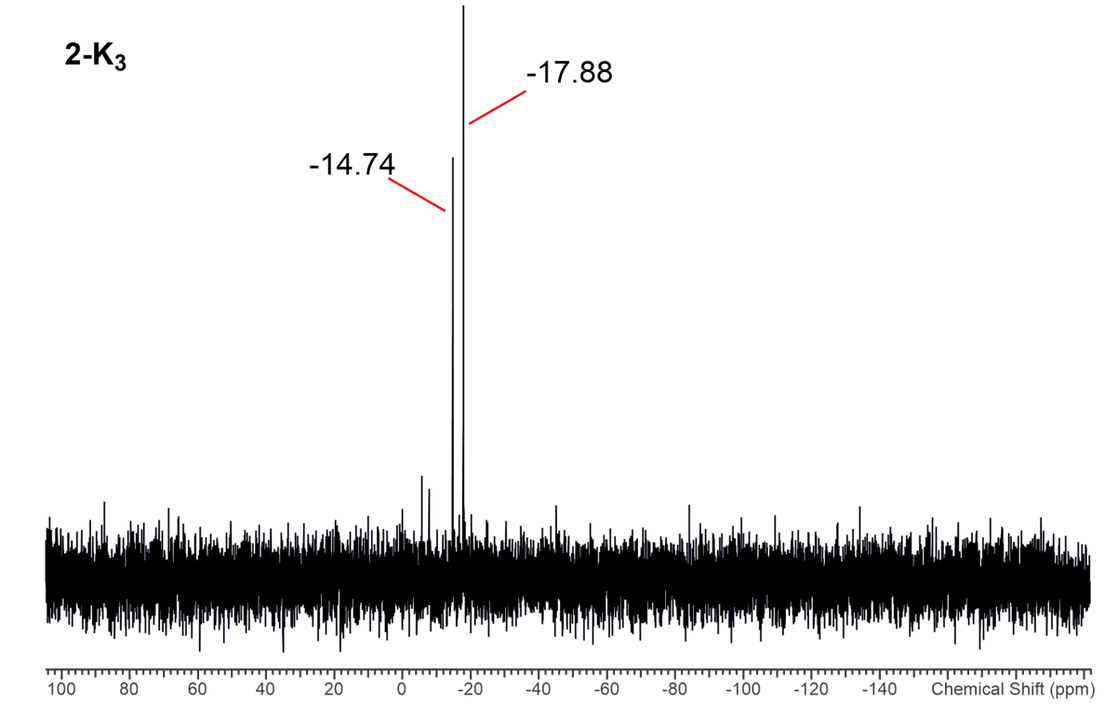

Figure S24. ^{29}Si DEPT NMR spectrum of **2-K$_3$** in C_4D_8O.

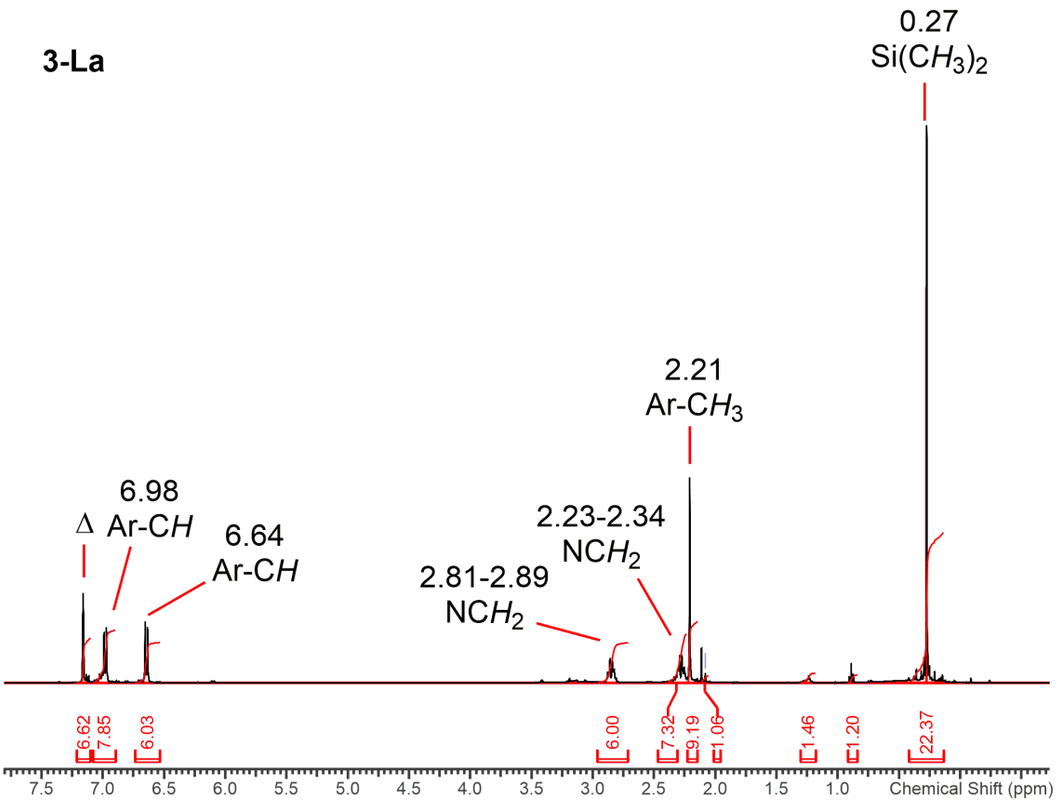

Figure S25. ^{1}H NMR spectrum of **3-La** in C_6D_6. Δ denotes C_6H_6.

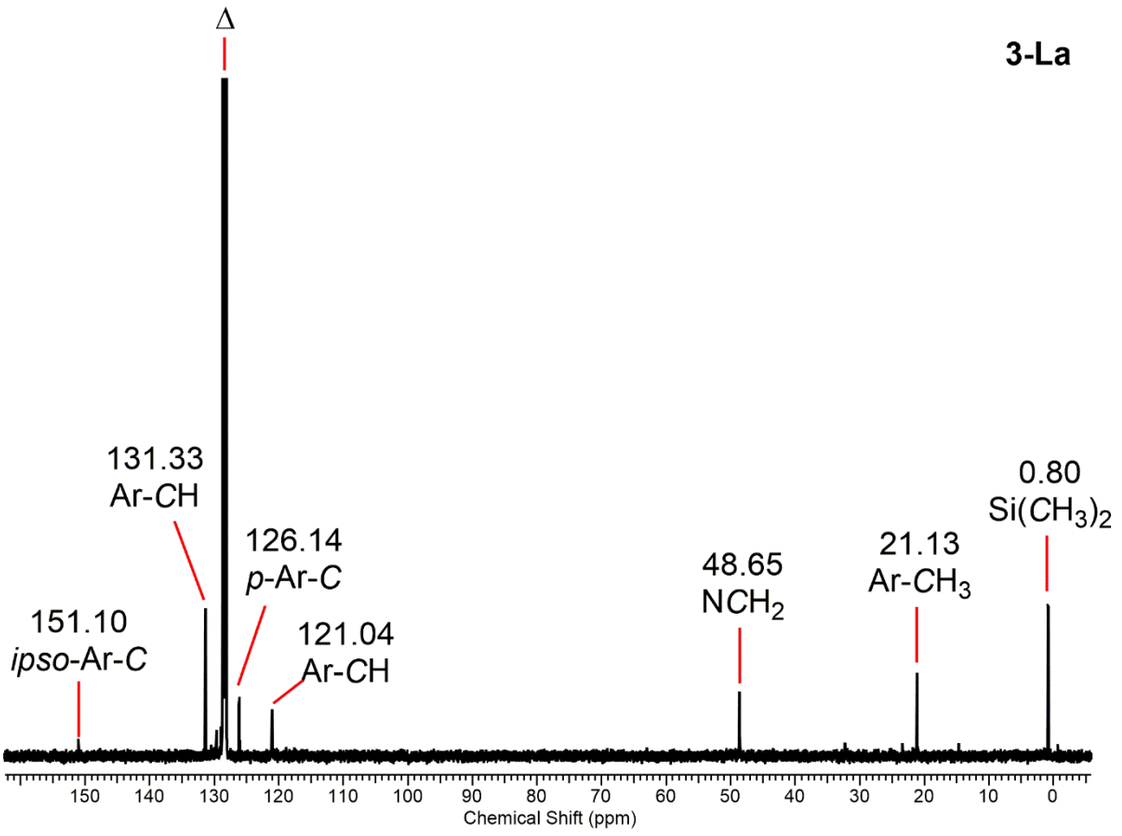

Figure S26. ^{13}C{^{1}H} NMR spectrum of **3-La** in C_6D_6. Δ denotes C_6H_6.

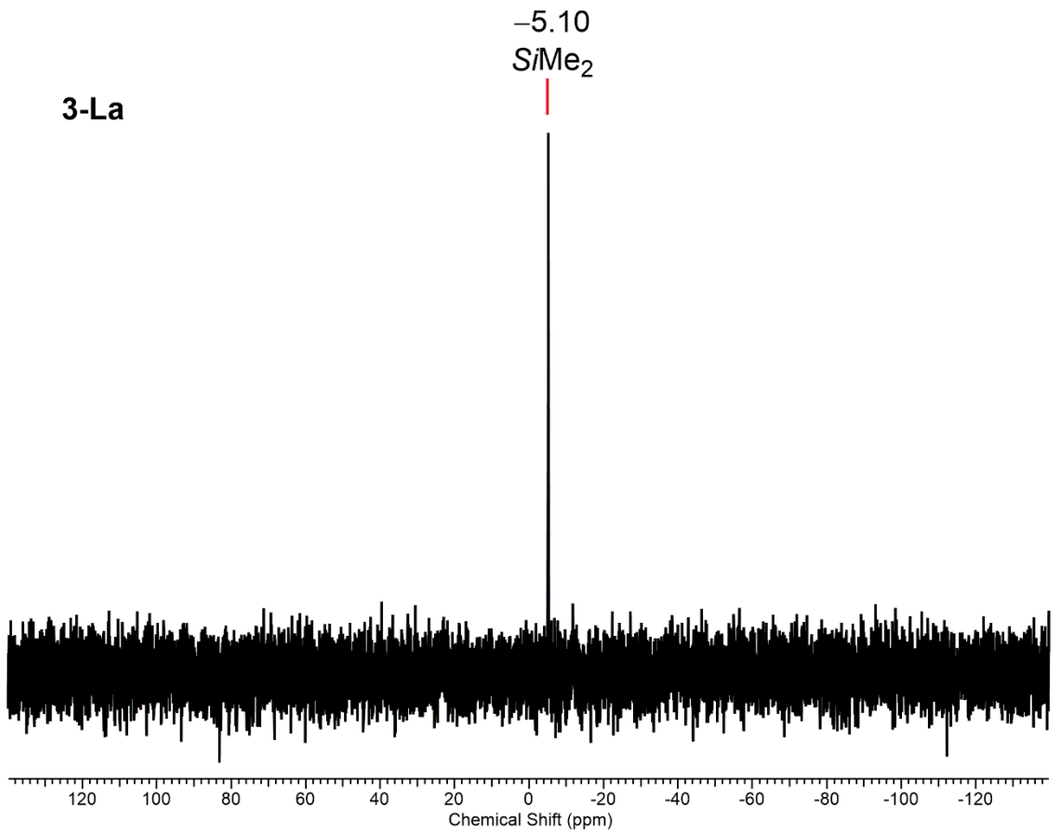

Figure S27. $^{29}Si\{^{1}H\}$ NMR spectrum of **3-La** in C_6D_6.

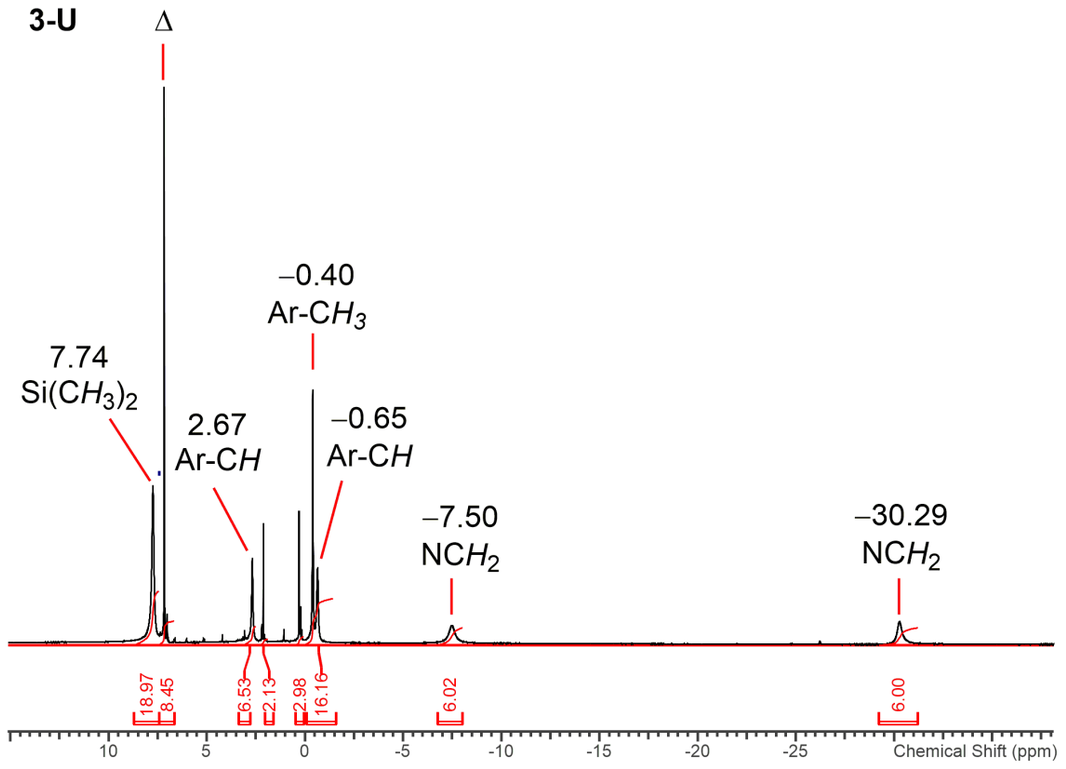

Figure S28. ^{1}H NMR spectrum of **3-U** in C_6D_6. Δ denotes C_6H_6.

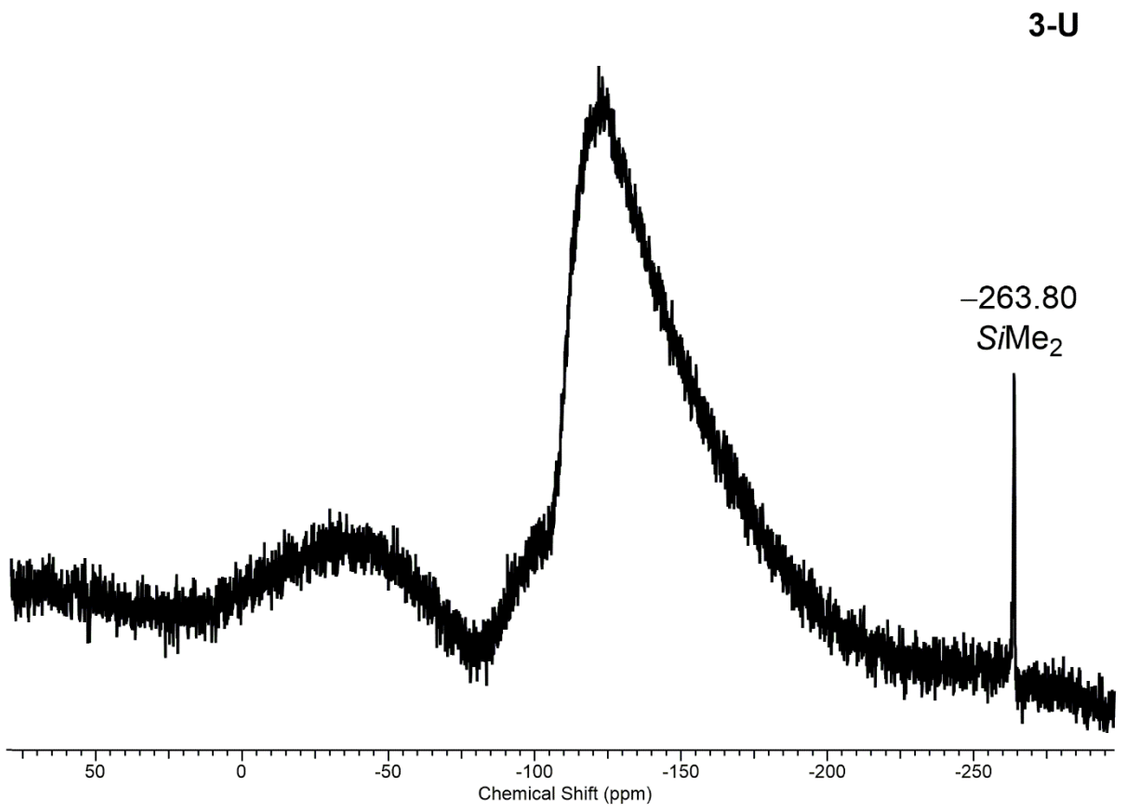

Figure S29. $^{29}Si\{^{1}H\}$ NMR spectrum of **3-U** in C_6D_6.

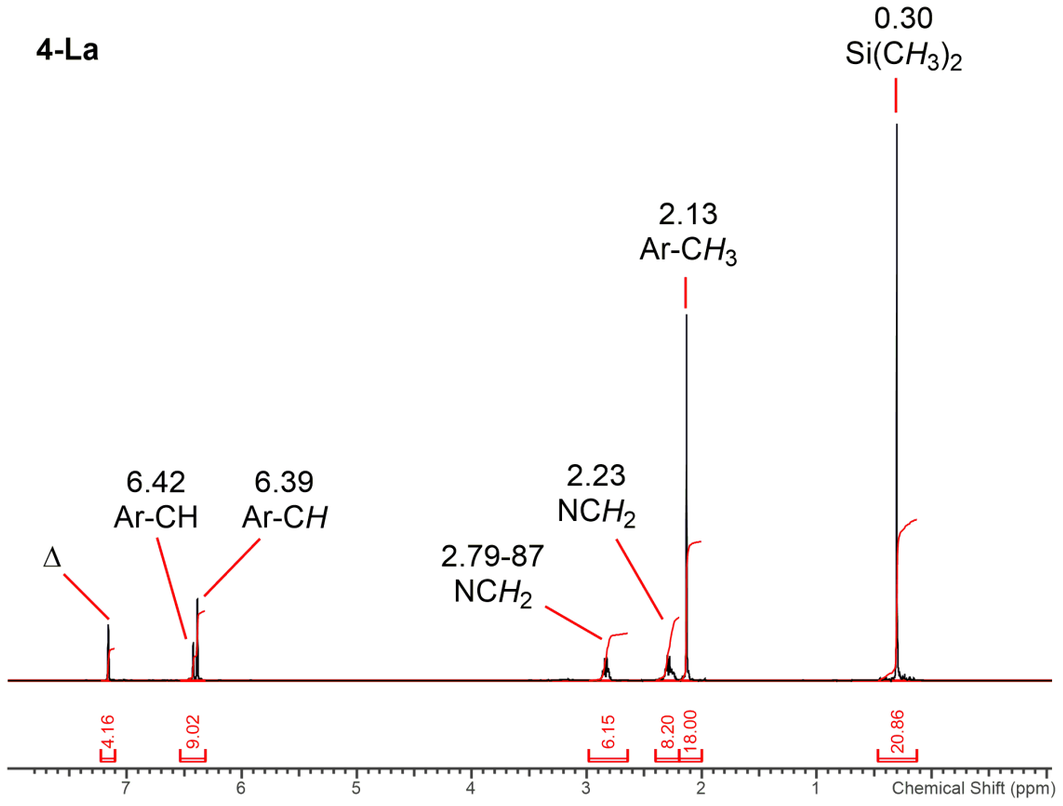

Figure S30. ^{1}H NMR spectrum of **4-La** in C_6D_6. Δ denotes C_6H_6.

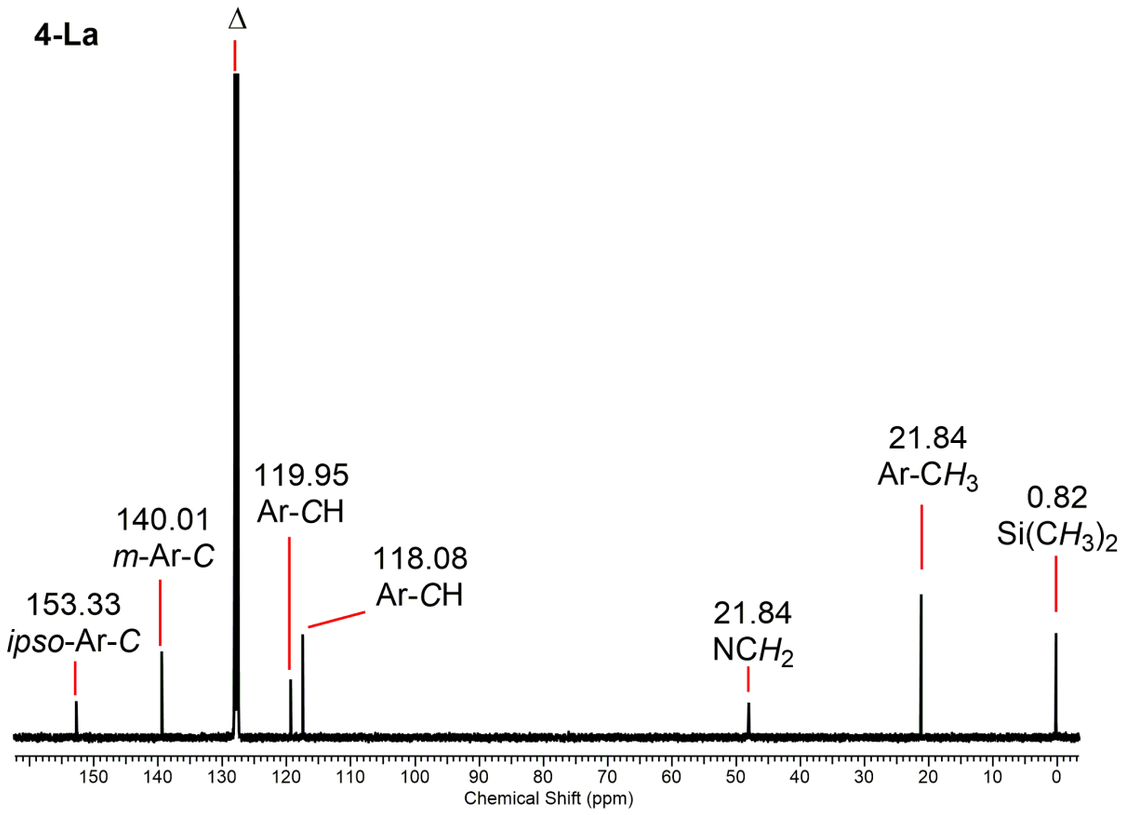

Figure S31. $^{13}C\{^{1}H\}$ NMR spectrum of **4-La** in C_6D_6. Δ denotes C_6H_6.

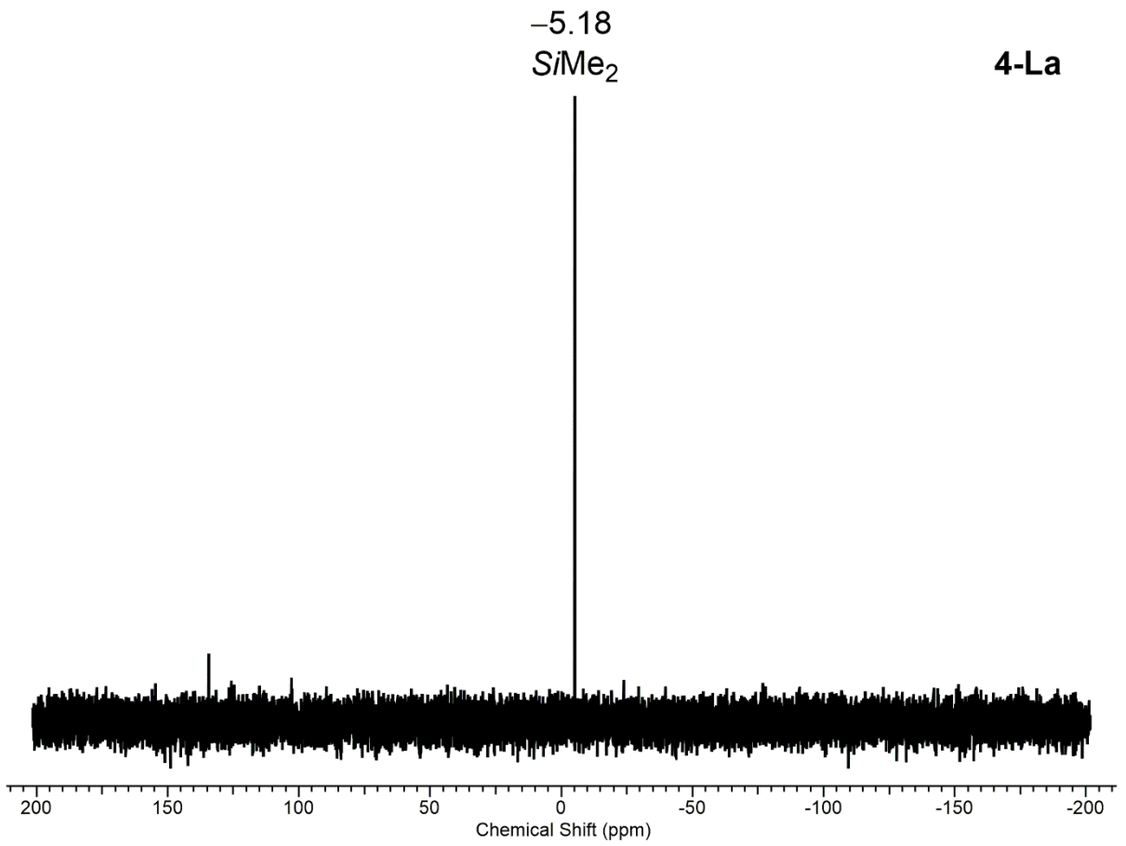

Figure S32. $^{29}Si\{^{1}H\}$ NMR spectrum of **4-La** in C_6D_6.

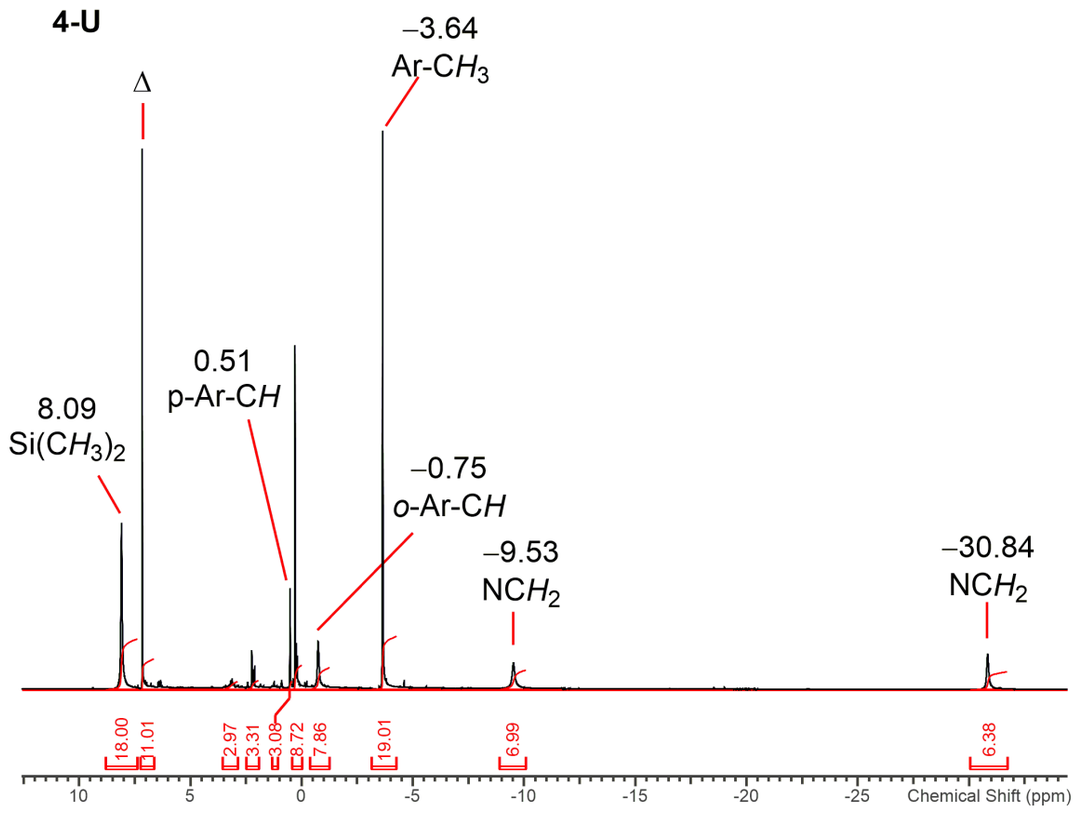

Figure S33. ^{1}H NMR spectrum of **4-U** in C_6D_6. Δ denotes C_6H_6.

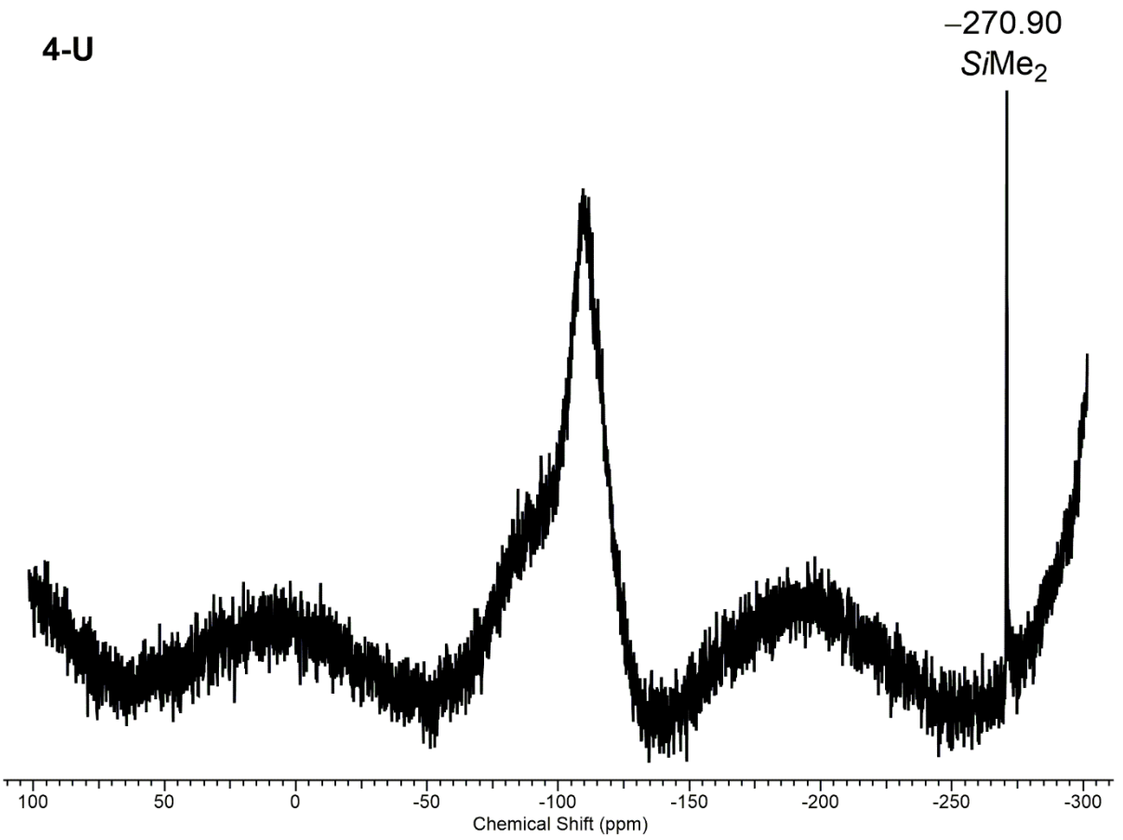

Figure S34. ^{29}Si{^{1}H} NMR spectrum of **4-U** in C_6D_6.

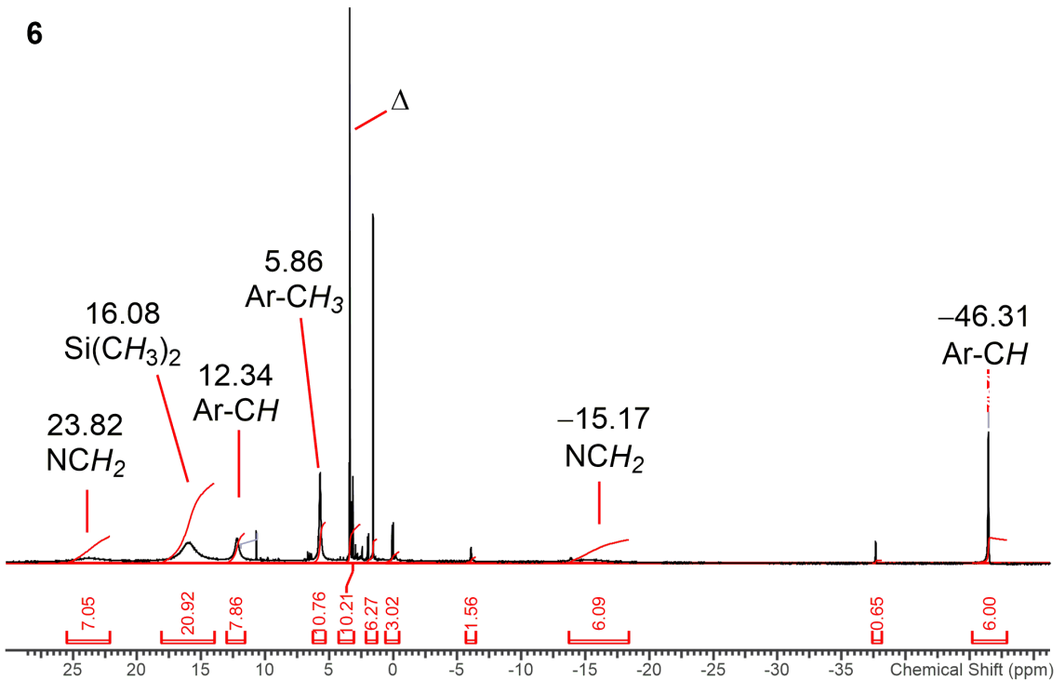

Figure S35. ^{1}H NMR spectrum of **6** in C_4D_8O, prepared by Method 1. Δ denotes C_4D_8O.

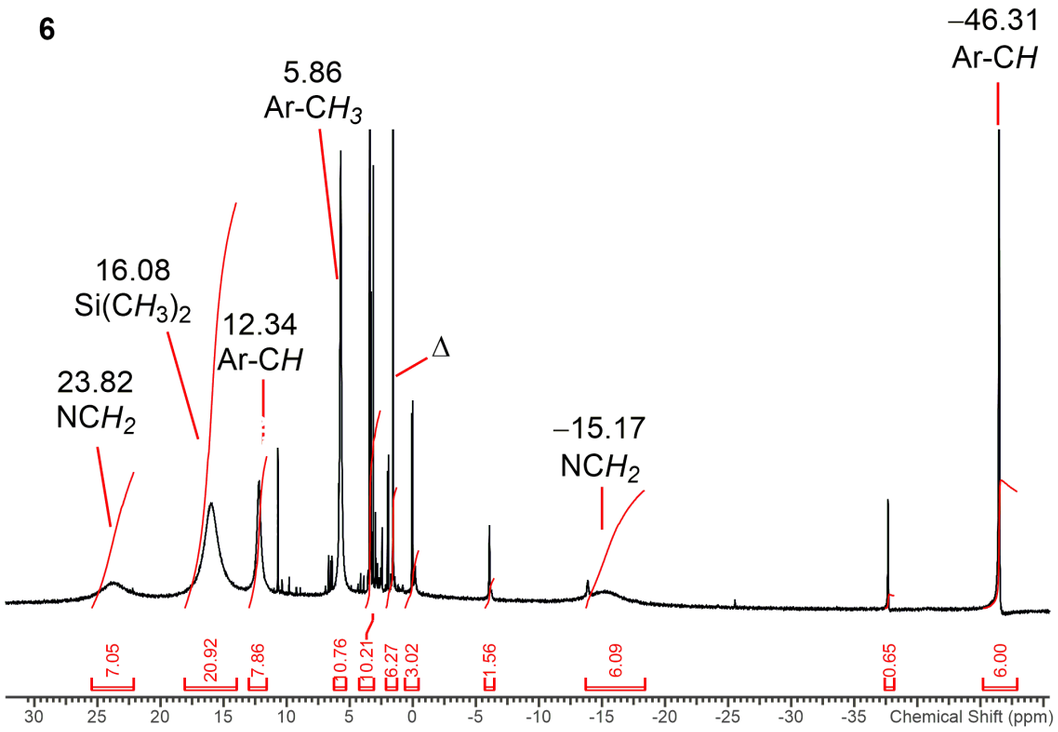

Figure S36. ^{1}H NMR spectrum of **6** in C_4D_8O, prepared by Method 1, zoomed in to show signals that are paramagnetically broadened into the baseline. Δ denotes C_4D_8O.

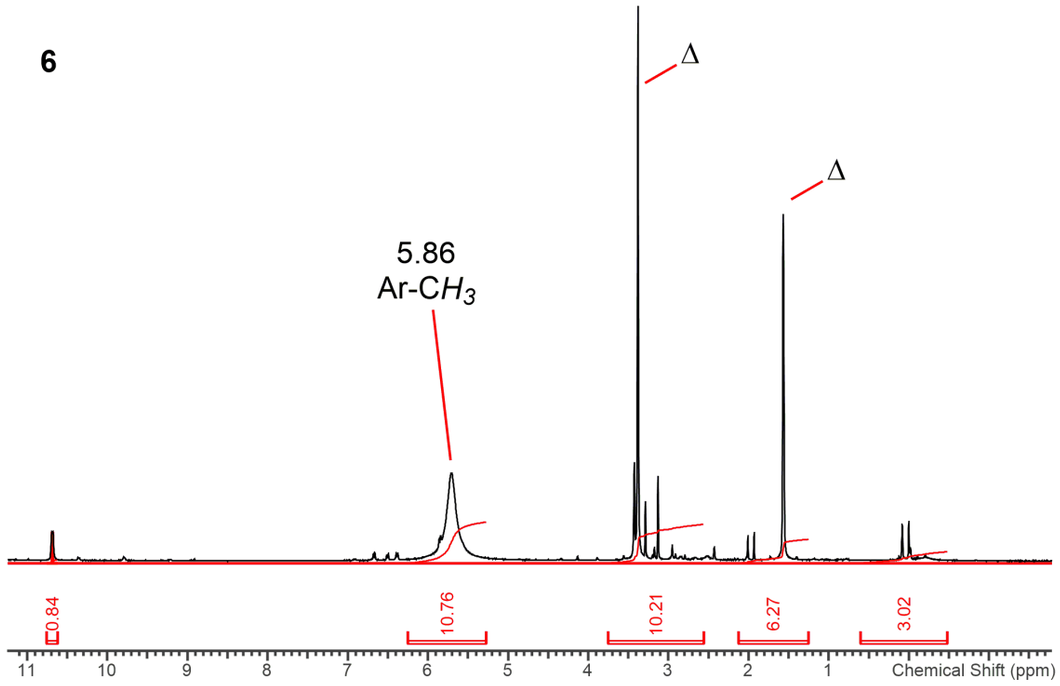

Figure S37. ^{1}H NMR spectrum of **6** in C_4D_8O, prepared by Method 1, zoomed in to show signals in the diamagnetic region. Δ denotes C_4D_8O.

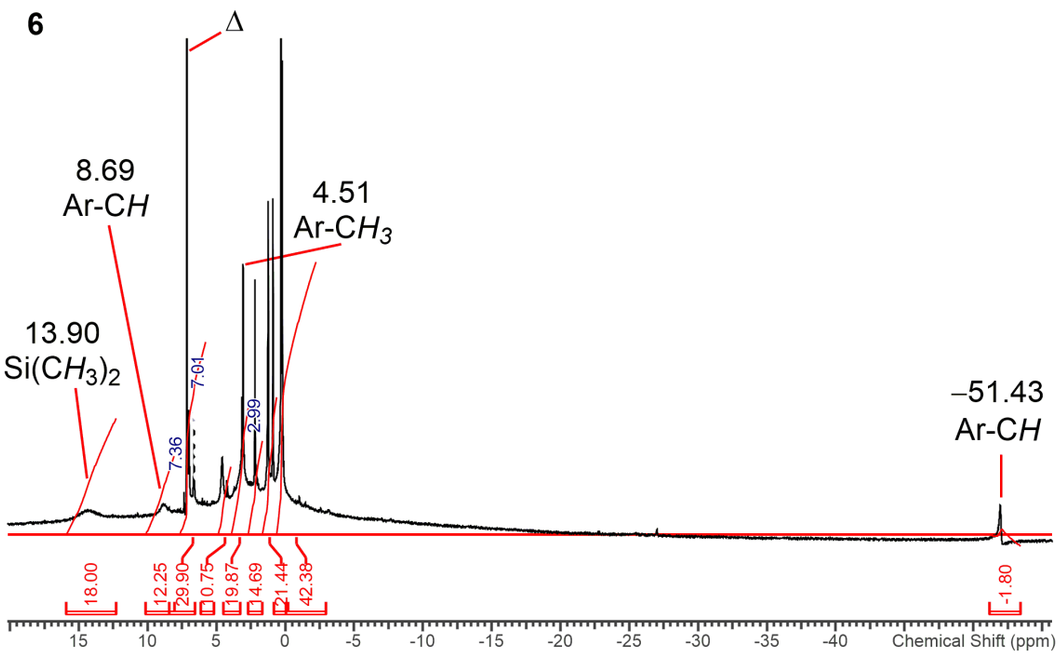

Figure S38. ^{1}H NMR spectrum of **6** in C_6D_6, prepared by Method 1. Δ denotes C_6H_6. Note that there are minor chemical shifts compared to the ^{1}H NMR spectra collected in C_4D_8O shown above, with the deshielded NCH_2 resonance not visible in C_6D_6.

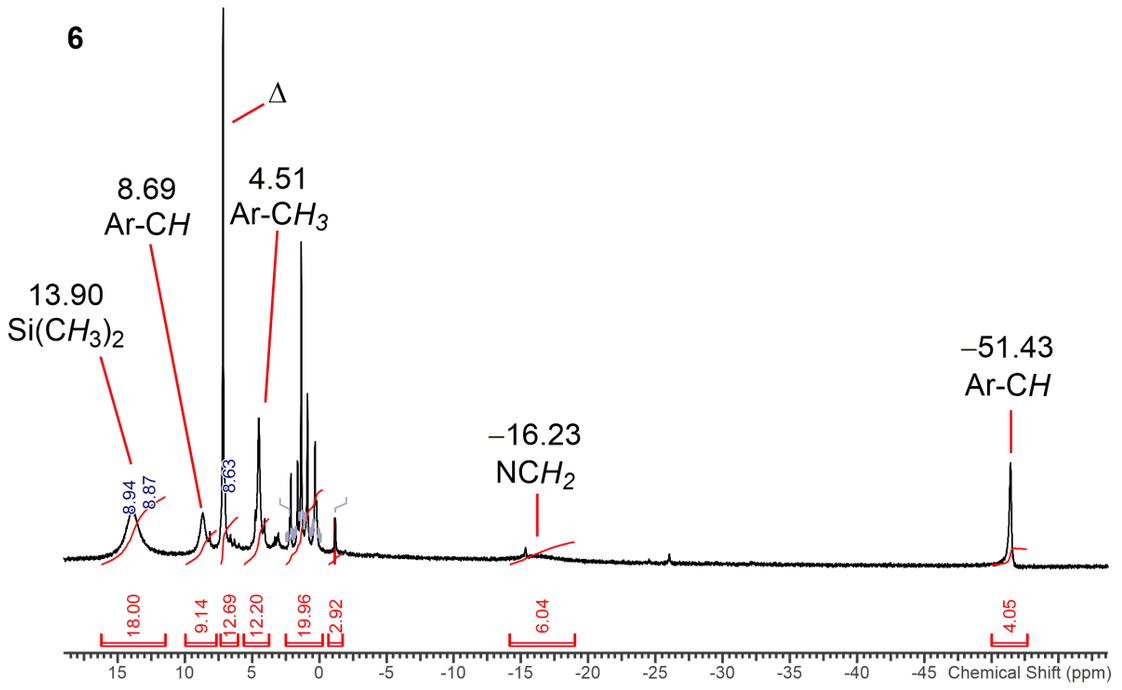

Figure S39. ^{1}H NMR spectrum of **6** in C_6D_6, prepared by Method 2. Δ denotes C_6H_6. Note that there are differences in the amount of diamagnetic impurities between Method 1 and Method 2, and unlike the spectrum above the shielded NCH_2 resonance is visible.

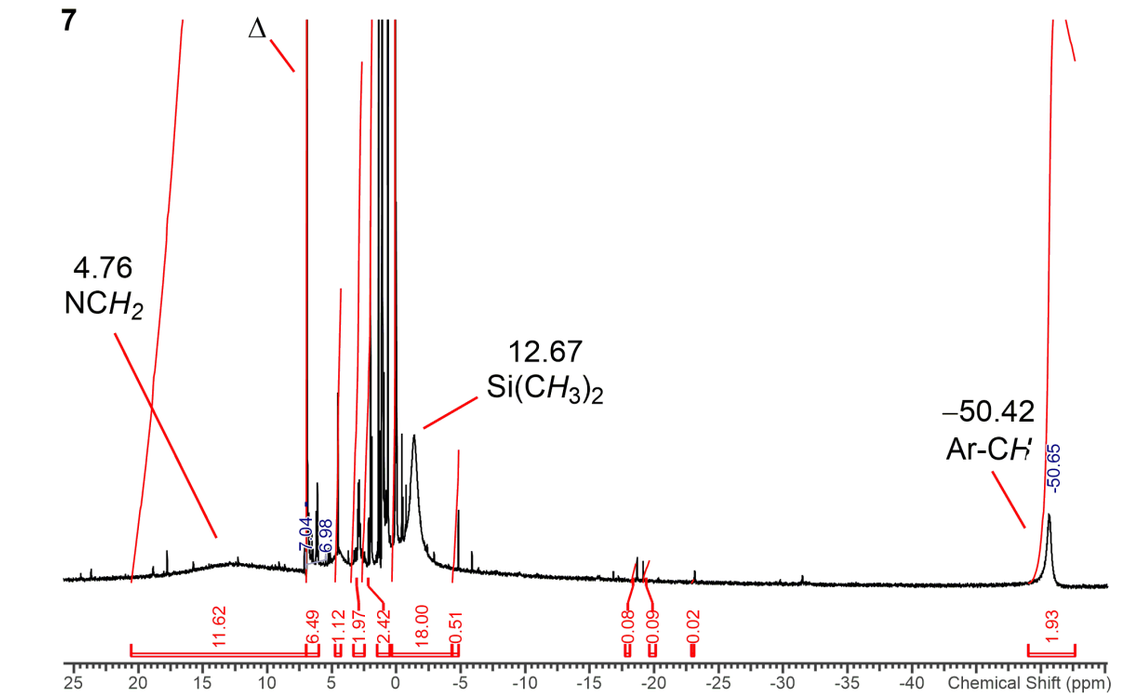

Figure S40. ^{1}H NMR spectrum of **7** in C_6D_6, prepared by Method 1. Δ denotes C_6H_6.

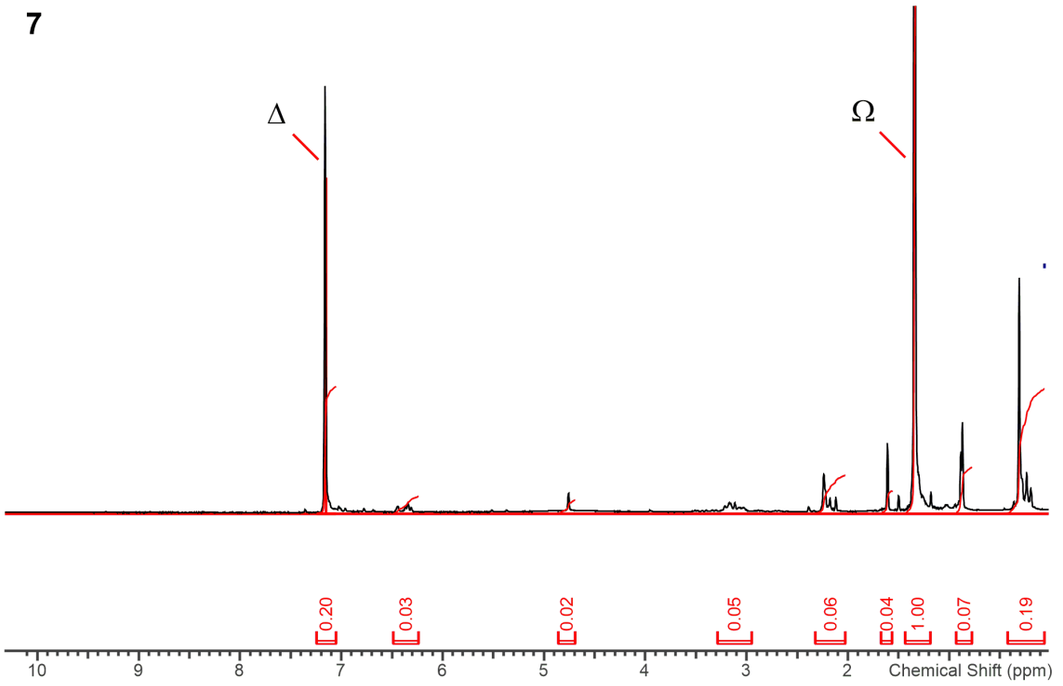

Figure S41. ^{1}H NMR spectrum of **7** in C_6D_6, prepared by Method 1, zoomed in to show signals in the diamagnetic region. Δ denotes C_6H_6, Ω denotes silicon grease.

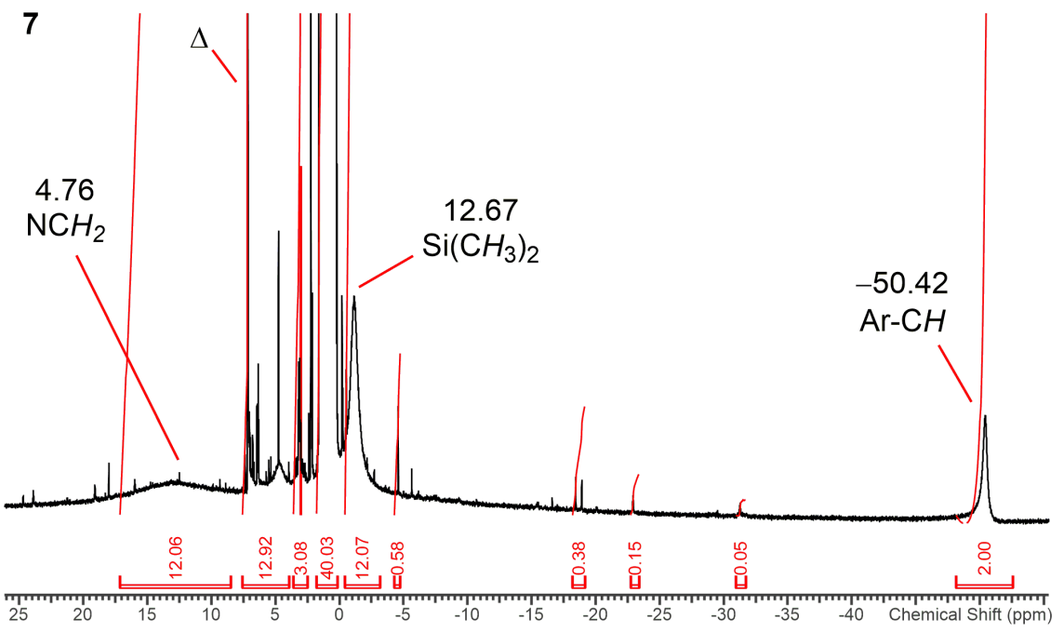

Figure S42. ^{1}H NMR spectrum of **7** in C_6D_6, prepared by Method 2. Δ denotes C_6H_6. Note that there are differences in the amount of diamagnetic impurities between Method 1 and Method 2.